

Large ensemble simulations of the North American and Greenland ice sheets at the Last Glacial Maximum with a coupled atmospheric general circulation-ice sheet model

Sam Sherriff-Tadano^{1,6}, Ruza Ivanovic¹, Lauren Gregoire¹, Charlotte Lang², Niall Gandy^{1, 5}, Jonathan Gregory^{2,3}, Tamsin L. Edwards⁴, Oliver Pollard¹ and Robin S. Smith²

¹ School of Earth and Environment, University of Leeds, UK

² National Centre for Atmospheric Science, University of Reading, UK

³ Met Office Hadley Centre, Exeter, UK

⁴ King's College London, UK

⁵ Department of Natural and Built Environment, Sheffield Hallam University, UK

⁶ [Department of Physics and Earth Sciences, University of the Ryukyus, Japan](#)

Correspondence to: Sam Sherriff-Tadano (tadanosam@gmail.com)

Abstract

The Last Glacial Maximum (LGM) ~~is was~~ characterised by huge ice sheets covering the Northern Hemisphere, especially over North America, and by its cold climate. ~~Numerical~~ [Previous authors have performed numerical](#) simulations of the ~~climate and ice sheets of the~~ LGM ~~have been performed~~ to better understand ~~these~~ [coupled climate - ice sheet](#) systems, ~~however the inherent uncertainty and sensitivity in the~~. [However, the results of such](#) simulations [are sensitive to the selection of many](#) model parameters ~~remain uncertain~~. Here, we perform a 200-member ensemble of simulations of the North American and Greenland ice sheets and climate of the LGM with an ice sheet-atmosphere-slab ocean coupled model (FAMOUS-BISICLES) to explore sensitivities of the coupled climate-ice system to 16 uncertain parameters. In the ensemble of simulations, the global [mean surface](#) temperature is primarily controlled by the combination of parameters in the large-scale condensation scheme and the cumulus convection scheme. In simulations with plausible LGM global [mean surface](#) temperatures, we find that the albedo parameters have only a small impact on the Greenland ice volume due to the limited area of surface ablation associated with the cold climate. Instead, the basal sliding law controls the ice volume by affecting ice transport from the interior to the margin. On the other hand, like the Greenland ice sheet in future climate change, the LGM North American ice sheet volume is controlled by parameters in the snow and ice albedo scheme. Few of our simulations produce an extensive North American ice sheet when the global temperature is above 12°C. Based on constraints on the LGM global [mean surface](#) temperature, the ice volume and the southern extent of the North American ice sheet, we select 16 acceptable simulations. These simulations lack the southern extent of ice compared to reconstructions, though show reasonable performance on the ice sheet configuration and ice streams facing the Baffin Bay and the Arctic Ocean. The strong sensitivities of the North American ice sheet to albedo at the LGM may imply a potential constraint on the future Greenland ice sheet by constraining the albedo schemes.

37 1. Introduction

38 The rise in sea level predicted in the next several centuries associated with increasing greenhouse gases and global warming
39 is one of the largest concerns of society and the climate [science](#) community. The most recent IPCC WG1 report projects a
40 global mean sea_level rise of more than 3 m under the high end ~~of the~~[SSP5-8.5 scenario for](#) increase in radiative forcing
41 ~~(SSP5-8.5)~~ in the next 300 years (IPCC 2021). However, there are still large uncertainties in ~~the predicted~~[projections of](#) sea
42 level rise with the possibility of a much larger magnitude (Edwards et al. 2021). This large uncertainty in the projection of
43 sea_level rise reflects the present limited state of knowledge of several important processes, such as nonlinear behaviours in
44 the ice sheet system ([e.g.](#) Gregoire et al. 2012, Abe-Ouchi et al. 2013, Golledge et al. 2019) and interactions of the climate
45 and the ice sheets, which are expressed in climate-ice sheet coupled models ([e.g.](#) Deconto and Pollard 2016, Golledge et al.
46 2019, Gregory et al. 2020, Smith et al. 2021). This uncertainty shows the importance of improving our understanding of the
47 ice sheet-climate coupled system and ~~to refine~~[refining](#) numerical models used for the future projection of climate and sea-
48 level rise.

49
50 One method of evaluating climate-ice sheet coupled models and improving understanding of the climate-ice sheet coupled
51 system is to simulate conditions of past periods. In this regard, the Last Glacial Maximum (LGM), which corresponds to
52 approximately 21 thousand years before present (ka BP; Clark et al. 2009, Kageyama et al. 2021), is useful since both
53 climate conditions and the ice sheet configurations are relatively well documented compared to previous periods of
54 glaciation (Tarasov et al. 2012, Kageyama et al. 2021). It has been suggested that the LGM could be used to constrain ~~the~~
55 climate sensitivity (Tierney et al. 2020), cloud processes (Zhu et al. 2022) and deep ocean circulation (Sherriff-Tadano et al.
56 2023), implying that understanding this period has the- potential to help constrain climate and ice sheet models and future
57 sea level projections. During this period, weaker summer insolation and lower concentrations of greenhouse gases caused the
58 climate to be colder, allowing ice sheets to expand over North America and Northern Europe. As a result, the global climate
59 was colder by 1.7°C to 8.3°C (Holden et al. 2010, Schmittner et al. 2011, Tierney et al. 2020, Paul et al. 2021) and global
60 mean sea level was approximately 120 m lower compared to modern (Clark et al. 2009, Gowan et al. 2021). The mass of the
61 Greenland ice sheet is thought to have been larger by approximately by 2 to 5 m sea level equivalent (SLE) at the LGM
62 (Clark and Mix 2002, Lecavalier et al. 2014, Bradley et al. 2018, Tabone et al. 2018) and of the Antarctic ice sheet by 5.6 to
63 14.3 m SLE ([e.g.](#) Briggs et al. 2014). The Eurasian ice sheet is thought to have attained a volume of 24 m SLE (Hughes et al.
64 2016), but by much the largest part of the 120 m SLE is attributed to the growth of the North American ice sheet (at least 60
65 m SLE, [e.g.](#) Abe-Ouchi et al. 2015). The position of the margin of the North American ice sheet is constrained reasonably
66 well by geological evidence and this line of evidence is often used to validate the performance of ice sheet models ([e.g.](#),
67 Dyke et al. 2002, Clark et al. 2009).

68
69 Studies that simulate LGM climate and ice-sheets have primarily treated these components independently using
70 ~~individual~~[separate](#) numerical models. To investigate the effect of ice sheets on climate, following Manabe and Broccoli
71 (1985), many simulations have been performed and compared ~~their simulations with climate models as part of the,~~ [including](#)
72 [in studies contributed to the long-running](#) Paleoclimate Model Intercomparison Project (PMIP, Braconnot et al. 2007, 2012,
73 Ivanovic et al. 2016, Kageyama et al. 2017). ~~In these simulations, the~~[The](#) ice sheet configuration was specified as a boundary
74 condition ~~and they~~[in these simulations, which](#) show the important role of the ~~existence of the glacial~~ ice sheets on ~~the~~[glacial](#)
75 climate, affecting surface temperature, precipitation, atmospheric and oceanic circulation ([Smith and Gregory, 2012;](#)
76 Klockmann et al. 2016, Gregoire et al. 2018, Ivanovic et al. 2018, Sherriff-Tadano et al. 2021). To investigate the effect of
77 climate on ice sheets, simulations of the LGM ice sheets have been performed with ice sheet models. ~~These simulations were~~
78 ~~performed,~~ either as full glacial cycle experiments ([e.g.](#) Abe-Ouchi et al. 2007) or [perpetual equilibrium](#) LGM experiments
79 ([e.g.](#) Alder and Hostetler 2019). In these experiments, the ice sheet models were forced with climatic conditions based on

80 outputs from general circulation models (Gregoire et al. 2012, Abe-Ouchi et al. 2013, Alder and Hostetler 2019, Niu et al.
81 2019, Blasco et al. 2021). They showed the critical effects of uncertain climatic conditions and albedo in causing a large
82 diversity in the simulated ice sheet configuration (Abe-Ouchi et al. 2007, Alder and Hostetler 2019, Niu et al. 2019, Blasco
83 et al. 2021) together with uncertainties in basal sliding law (Gandy et al. ~~2020~~2019). These studies highlighted the strong
84 interaction of climate and ice sheets and the importance of performing simulations with climate-ice sheet coupled models to
85 better understand the coupled system.

86

87 Recent efforts in the modelling community in developing complex coupled climate-ice sheet models (e.g. Gregory et al.
88 2012, Ziemen et al. 2014, Roche et al. 2014, Smith et al. 2021) mean that higher complexity coupled climate-ice simulations
89 of the glacial period than have previously been possible may now be performed. Gregory et al. (2012) performed simulations
90 of an ice sheet inception over North America with the climate-ice sheet coupled model FAMOUS-Glimmer. They showed
91 the role of the albedo on the magnitude and speed of the inception. Ziemen et al. (2014) performed simulations of the ice
92 sheet-atmosphere-ocean system with a more complex ice sheet-climate coupled model. Their simulation reproduced the
93 climate and the ice sheets of the LGM reasonably well, while the southern extent of the North American ice sheet was
94 somewhat smaller compared to reconstructions. This is partly due to the relatively coarse resolution of the atmospheric
95 model (Ziemen et al. 2014), which means their model underestimated the stationary wave effect that cools the southern
96 extent of the North American ice sheet and hence underestimates the ice area in that region (Roe and Lindzen 2001, Abe-
97 Ouchi et al. 2007). Lofverstrom et al. (2015) performed simulations of the North American ice sheet and climate with an
98 atmosphere-ice sheet-slab ocean coupled model in an idealised framework and showed the importance of interactions
99 between atmospheric circulation, the Rocky Mountains and the ice sheet in shaping the ice sheet's zonally asymmetric
100 features. Willeit and Ganopolski (2016) presented simulations of the last glacial cycle with an ice sheet model coupled to an
101 Earth System model of intermediate complexity and discussed the role of the darkening effect of snow. Quiquet et al. (2021)
102 performed simulations of the ice sheets and climate of the LGM and the last deglaciation with a coupled climate-ice sheet
103 model. They managed to reproduce the overall characteristics of the evolution of climate and ice sheets and showed the
104 effects of modulations in the oceanic circulation.

105

106 These previous studies provide very useful insight into the physical interactions within the coupled system, but the inherent
107 uncertainty and sensitivity in the simulations to the selection of model inputs (including physical parameterisations) remain
108 untested as are not tested in all any of these studies, because they each use a single version of a given model was used.

109

110 Perturbed parameter ensembles of simulations are a powerful way to estimate uncertainties originating from particular
111 parameter values in a single model (Murphy et al. 2004, Sanderson 2011, Shiogama et al. 2012). For example, Rougier et al.
112 (2009) analysed results from an ensemble performed under modern and future climate conditions with an atmosphere-slab
113 ocean coupled general circulation model (HadSM3) and showed the critical role of entrainment rate in the cumulus cloud
114 scheme and its interaction with large-scale condensation scheme on global climate. Gregoire et al. (2011) performed an
115 ensemble of simulations with an atmosphere-ocean coupled general circulation model, FAMOUS, and found that the mid-
116 latitude cloud parameters and sea ice albedo exert an important influence on global cooling at the LGM. Furthermore, they
117 used their results to identify combinations of parameter values that optimise model skill in simulating both the pre-industrial
118 and LGM, thus improving model flexibility. Gandy et al. (2023) recently performed ensemble simulations of the North
119 American ice sheet and climate with an atmosphere-ice sheet coupled model FAMOUS-Ice (Smith et al. 2021). They
120 showed the importance of ice and snow albedo in building the ice sheet due to strong summer insolation at the southern
121 margin of the North American ice sheet. In this study, however, the sea surface temperature and the global temperature were

122 fixed. As a result, the role of clouds on the climate and the effects of global mean [surface](#) temperature ([GMST](#)) on the ice
123 sheet volume ~~remained unclear~~[could not be examined](#).

124
125 Here, we perform a large ensemble of simulations of the North American and Greenland ice sheets and climate of the LGM
126 with a version of the FAMOUS-Ice coupled atmosphere-ice sheet model, ~~which utilises the~~[including a more sophisticated](#)
127 ice sheet model, BISICLES ~~rather than Glimmer~~ (Method, e.g. Smith et al. 2021). With this [model ensemble](#), we estimate
128 the impact of uncertainty in the choice of parameter values implemented in the atmosphere and ice sheet components of the
129 model, and [we](#) test the ability of the model to simulate ice sheets and climates very different from today. The results are
130 evaluated against the LGM ~~global mean temperature~~[GMST](#), ice volume and southern extent of the North American ice sheet.
131 Through these experiments, we aim to address the following questions:

- 132 • How do uncertain parameters affect the climate and ice sheets at the LGM?
- 133 • Is there a difference in important parameters between the North American and Greenland ice sheets?
- 134 • How well are the ice sheets simulated in this experiment, e.g. in terms of North American ice sheet volume, the
135 southern extent of the North American ice sheet and the position of the ice streams?

136
137 The remainder of the paper is structured as follows. Section 2 gives a description of the model, the experimental design and
138 the integration procedure. Section 3 reports on the results of the large ensemble. Section 4 discusses the results and the effect
139 of biases in the model. Lastly, section 5 gives the conclusions.

141 2. Method

142 2.1 Model

143 Our simulations of the climate and ice sheets are performed with the atmosphere-ice sheet-slab ocean coupled model,
144 FAMOUS-Ice (Smith et al. 2021, Gregory et al. 2020). FAMOUS is a low-resolution version of the atmosphere-ocean
145 general circulation model (AOGCM) HadCM3; the horizontal resolution is 7.5° in longitude and 5° in latitude (Smith et al.
146 2008, 2012). Due to the lower resolution, FAMOUS runs 10 times faster compared to HadCM3, while retaining a reasonable
147 performance for the modern and the LGM climates (Smith et al. 2008, 2012, Smith and Gregory 2012). Benefitting from
148 much cheaper computational cost, it is feasible to run multi-millennial simulations (Smith and Gregory 2012; [Gregory et al.](#)
149 [2020](#)) and large ensembles (Gregoire et al. 2011), as required to meet our objectives.

150
151 The latest version of FAMOUS (FAMOUS-~~ice~~[Ice](#), Smith et al. 2021) incorporates a downscaling scheme for the calculation
152 of the surface mass balance (SMB) over ice sheets. In the downscaling scheme, 10 additional vertical tiles are added to better
153 represent the elevation dependence of surface temperature and downward longwave radiation, following the method first
154 used in Vizcaino et al. (2013). The downscaled temperature and longwave radiation are then utilised with downward
155 shortwave radiation to calculate the SMB based on a surface energy budget [and a multi-layer snow](#) scheme, together with
156 precipitation from the original FAMOUS grid. The model also incorporates an updated snow and ice albedo scheme, which
157 accounts for albedo changes associated with modifications in surface air temperature (*daice*), grain size (*avgr*) and density of
158 the snow (*fsnow*) (Smith et al. 2021, Table 1). As a result, the atmospheric model reproduces the general pattern of SMB
159 over the modern Greenland ice sheet reasonably well (van de Wal et al. 2012, Smith et al. 2021) with some ~~overestimating~~
160 ~~biases in~~[overestimation of](#) the elevation of Equilibrium-Line Altitude (ELA; Smith et al., 2021, see also subsection 4.23).

162 Previous work with FAMOUS-~~ice~~Ice used prescribed climatological SSTs and sea-ice instead of an interactive ocean model
163 (Gregory et al., 2020; Smith et al., 2021, Gandy et al. 2023). In the present study, we use a slab ocean model with the same
164 horizontal resolution as the atmosphere. Inclusion of a slab ocean model allows the local and global SST and sea-ice to vary
165 in response to changes in climate, which in our experiments are caused by modifications in parameters and the advance and
166 retreat of ice sheets. In the slab ocean model, sea-ice is advected by the climatological monthly surface sea-water velocity of
167 the HadCM3 pre-industrial control experiment, with sea-ice convergence prevented when the local thickness exceeds 4.0 m.
168 The local thickness of sea ice evolves due to snowfall, sublimation and melting at the surface, and melting and freezing at
169 the base in response to heat exchange with the slab ocean. The SST is the temperature of a layer of water 50 m thick, and
170 evolves in response to surface energy exchange with the atmosphere and heat transport within the slab ocean. Since the slab
171 ocean does not simulate ocean dynamics, climatological heat transport is prescribed within it as a monthly climatological
172 field of heat convergence. The heat convergence field is obtained from a calibration experiment (Section 2.2) in which the
173 model calculates the heat flux necessary to maintain a reference climatological state of SST and sea-ice.

174
175 The slab ocean model is essentially the same as described by Williams et al. (2001), where it is used with the HadCM3
176 AGCM, but the present study is the first to use it with the atmosphere resolution of FAMOUS. For this configuration, grid
177 boxes which are partly land and partly sea were implemented in the slab ocean, as in the AGCM. In order to prevent unstable
178 surface temperature feedbacks in coastal grid boxes with small sea fraction, we found that horizontal diffusion of heat in the
179 slab ocean was needed (diffusivity $10000 \text{ m}^2 \text{ s}^{-1}$); unlike the prescribed heat convergence, diffusive heat divergence responds
180 to the time-dependent slab temperature gradient and thus dissipates local anomalies, but usually it is much smaller than the
181 heat convergence. In order to prevent local build-up of excessively thick coastal sea ice, we allow horizontal diffusion of sea
182 ice thickness (diffusivity $5000 \text{ m}^2 \text{ s}^{-1}$) when the local thickness exceeds 4.0 m. To improve the reproduction of the reference
183 sea-ice climatology, we adjusted the coefficients for sea-ice basal melting.

184
185 Instead of ~~the Glimmer, ice sheet model which was used in the previous studies of FAMOUS-Ice~~ (Gregory et al., 2020;
186 ~~Smith et al., 2021, Gandy et al. 2023~~), we use the more complex and computationally demanding BISICLES ~~ice sheet~~-model
187 (Cornford et al. 2013) ~~for the ice sheet component of FAMOUS-Ice (hereafter referred to as FAMOUS-BISICLES)~~.
188 BISICLES is a vertically integrated ice sheet model, which has been mainly used for simulations of modern and future
189 Greenland (Lee et al. 2015, Smith et al. 2021b) and Antarctica (Martin et al. 2019, Smith et al. 2021b), and has recently been
190 ~~applied for reproducing~~used to simulate past ice sheets over North America (Matero et al. 2020) and Northern Europe
191 (Gandy et al. 2018, 2019, ~~2020~~2021). Whereas Glimmer uses the shallow ice approximation, BISICLES applies a L1L2
192 approximation, which allows more flexibility in sliding and flowing of the ice sheet especially at the ice shelf area (Cornford
193 et al. 2013). In addition, the model is capable of changing spatial resolution according to the flow regime of the ice. In this
194 study, a horizontal ~~base~~ resolution of 32 km is chosen, with refinement to 16 km at ice sheet margins. The choice of the
195 resolution was made based on practical reasons regarding the computational expense. We show- that this resolution is
196 adequate for simulating large-scale glaciers in the northern area of the North American ice sheet (see subsection 4.~~4~~2).

197
198 We utilise a basal drag scheme introduced by Gandy et al. (2019), which explicitly expresses the thermodynamic interaction
199 of the ice sheets and the underlying till. This scheme combines the Coulomb-friction law and Weertman-friction law
200 depending on the water pressure in the bedrock sediment (Tsai et al. 2015). The basal drag follows the Weertman law under
201 cold ice basal temperature and dry bedrock sediment. Under warm ice basal temperature and wet bedrock sediment, the basal
202 drag follows the Coulomb-friction law. Depending on the depth of till water in the sediment, the friction of ice and bedrock
203 changes. The depth of the till water is controlled by the balance of basal melting of the ice sheet and a parameter (*drain*) that

204 controls the vertical till-stored drainage rate. Using this basal scheme in BISICLES simulations, Gandy et al. (2019)
205 reproduced the features of known ice streams in the LGM British ice sheet.

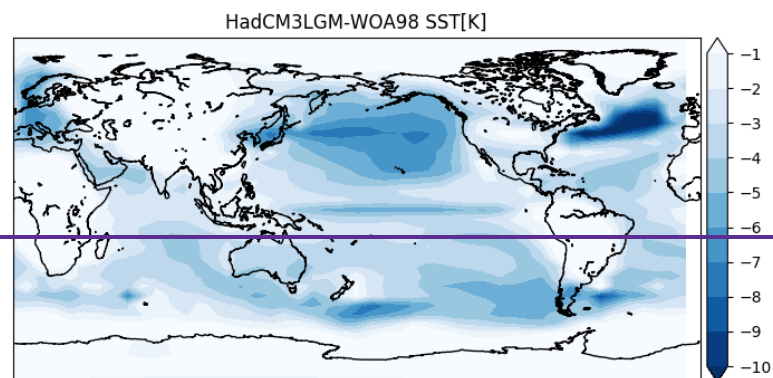
206
207 Changes in ice-sheet geometry, and the subsequent redistribution of the Earth's surface mass load, result in deformation of
208 the Earth's topography through a series of interconnected processes known as glacial isostatic adjustment (GIA). An
209 important impact of GIA for the purpose of ice-sheet modelling is the subsidence of the bedrock topography beneath an ice-
210 sheet. The rate of the solid Earth response towards isostatic equilibrium, which can range from centuries to millions of years,
211 is viscoelastic in nature as a result of the rheological structure of the Earth and specific pattern of ice loading. In order to
212 simulate the first-order effects of GIA on bedrock topography, we couple the ice-sheet model to a simple Elastic Lithosphere
213 Relaxing Asthenosphere (ELRA) model which approximates this response by assuming a fully elastic lithosphere above a
214 uniformly viscous asthenosphere (Kachuck et al. 2020). A relaxation time of 3000 years is applied in this model based on
215 previous studies (Pollard and Deconto 2012).

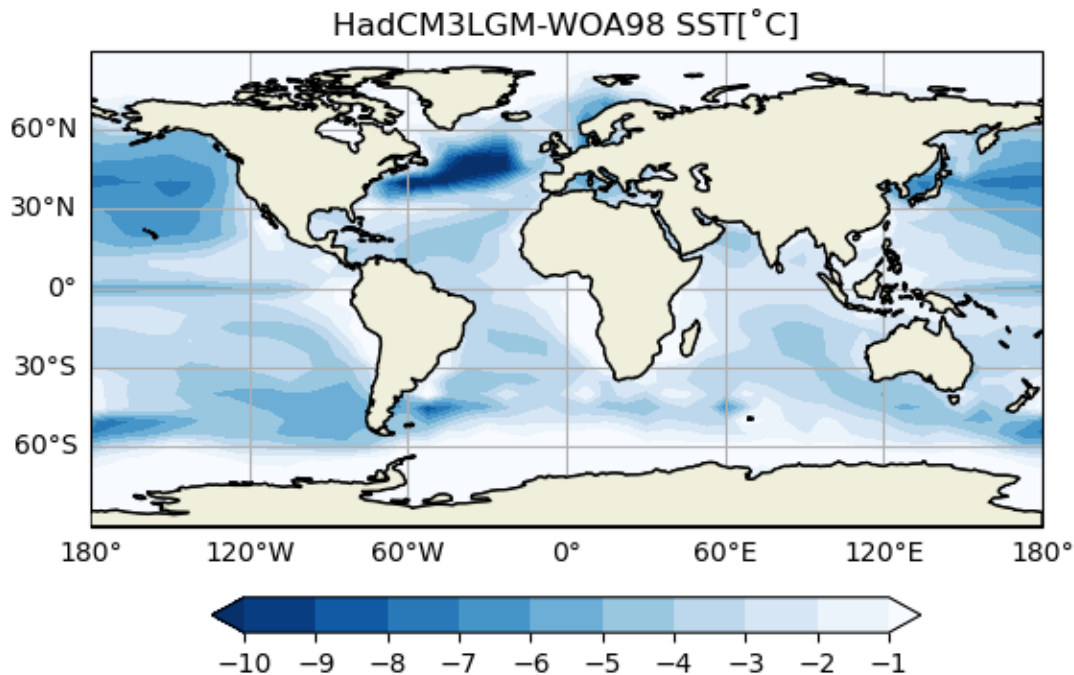
216
217 In running FAMOUS-BISICLES, a 10 times acceleration is applied to the ice sheet model to save computational cost
218 (Gregory et al. 2012, Ziemen et al. 2014). In this method, the ice sheet model is integrated for 10 years using for every 1-
219 year of climate simulation by FAMOUS. Gregory et al. (2012) and Gregory et al. (2020) show that 10 times acceleration has
220 a small to negligible impact on the simulated ice sheet evolution in FAMOUS, supporting the use of this technique.

221 2.2 Experimental design

222 Our experiments mainly follow the protocol of PMIP4 LGM simulations (Kageyama et al. 2017, 2021), which specifies the
223 insolation, atmospheric concentration of Greenhouse gases (CO₂=190 ppm, CH₄=375 ppb, NO₂=200 ppb, all by volume) and
224 configurations of continental ice sheets. With respect to ice sheets, in our setup, only theThe Eurasian and
225 AntarcticaAntarctic ice sheets are fixed to the reconstruction of GLAC-1D (~~Tarasove~~Tarasov et al. 2012) as in our setup,
226 while the LaurentideNorth American and Greenland ice sheets are simulated with BISICLES. While the protocol specifies
227 the insolation forcing of 21 ka BP, here we use the insolation of 23 ka since the ice sheet at the LGM is likely still adjusting
228 to earlier forcing (Abe-Ouchi et al. 2013).

229
230 For calibrating the slab ocean heat convergence (Section 2.1), we use the SST and sea-ice climatology from a previous LGM
231 simulation performed with HadCM3, shown in Fig. 1 (Izumi et al., 2023). ~~Their 2022~~ The simulated SST fieldGMST
232 exhibits a cold LGM climate, having a global cooling of 6.5 K. This value is similar to Tierney et al. (2020), who estimate
233 6.5 K to 5.7 K. For simplicity of design and clarity of interpretation, the oceanic heat flux is fixed among all the ensemble
234 simulations, thus assuming no changes in the oceanic heat transport in response to the different parameter values in each
235 member.





238

239 Fig. 1 Annual mean sea surface temperature anomaly fields (K, colour) between a HadCM3 LGM simulation and modern
 240 observation (World Ocean Atlas 1998). The sea surface temperature field from HadCM3 is used as the target sea surface
 241 condition for our prescribed slab ocean setup.

242

243 We perform 200-member ensemble simulations by [varying 16](#) varying 16 parameter values associated with climate and ice
 244 dynamics, as summarised in Table 1, using a Latin-hypercube sampling method (Williamson 2015), [assuming a uniform](#)
 245 [value probability across each parameter range, in order to explore the full ranges of the 16-dimensional parameter space. The](#)
 246 [Latin-hypercube sampling technique is useful as it allows exploration of all the uncertain parameter spaces in an efficient](#)
 247 [way. While some cancellations among parameters can cause lower correlation values between inputs and outputs, the](#)
 248 [method also provides quantitative insights on the complex interactions among different parameters \(e.g. Fig. 6 and Fig. S7 in](#)
 249 [this study\).](#)

250

251 The choice and the range of the parameter values in FAMOUS are modified following Gregoire et al. (2012) and Gandy et
 252 al. (2023). In BISICLES, the range of sliding law parameters are modified following sensitivity experiments of Gandy et al.
 253 (2019). For *drain*, which specifies the vertical till-stored drainage rate, the value is very uncertain and hence we varied it to
 254 ensure that the till of the interior of the ice sheet remains dry. Much lower values for *drain*, as used in Gandy et al. (2019) in
 255 their simulation of the much smaller British-Irish ice sheet, result in unphysically wet basal conditions and fast sliding in our
 256 simulations so we used a higher range. For *n*, which specifies the coefficient in Glen's flow law, the range is selected in a
 257 practical way; applying a high value increases the calculation time by more than 10 times due to very large ice velocities and
 258 the resulting refinement in several locations. Hence, the range of *n* is necessarily capped for its upper limit at 3.1, where our
 259 technical tests indicated that the simulations will most likely complete within a feasible run length (two months of wallclock
 260 time). During the ice sheet spin-up phase (see subsection 2.3) we specify a constant SMB. The value of this *smb* is varied

261 across the ensemble so that the ice volume at the initiation of FAMOUS-BISICLES coupling has a spread of 25 m SLE,
 262 which is similar to the uncertainty in the global ice volume estimates at the LGM (e.g. Abe-Ouchi et al. 2015). ~~For~~
 263 ~~simplicity, we apply spatially uniform basal heat fluxes of 158 mW/m² and 100W/m² under the grounded and floating ice~~
 264 ~~respectively, without testing other values. However, these choices need to be reassessed in the future, because the basal heat~~
 265 ~~flux over both the continent (e.g. Margold et al. 2018) and the ocean can vary spatially. Two hundred sets of parameter value~~
 266 ~~combinations for these 16 parameters are sampled using a Latin hypercube sampling method, assuming a uniform value~~
 267 ~~probability across each parameter range, to explore across the full ranges of the 16-dimensional parameter space.~~

268
 269 ~~For simplicity, we apply a single value, spatially uniform basal heat flux of 158 mW/m² and 100W/m² under the grounded~~
 270 ~~and floating ice respectively. However this needs to be reassessed in the future as both the basal heat flux over the continent~~
 271 ~~(e.g. Margold et al. 2018) and the ocean can vary spatially.~~

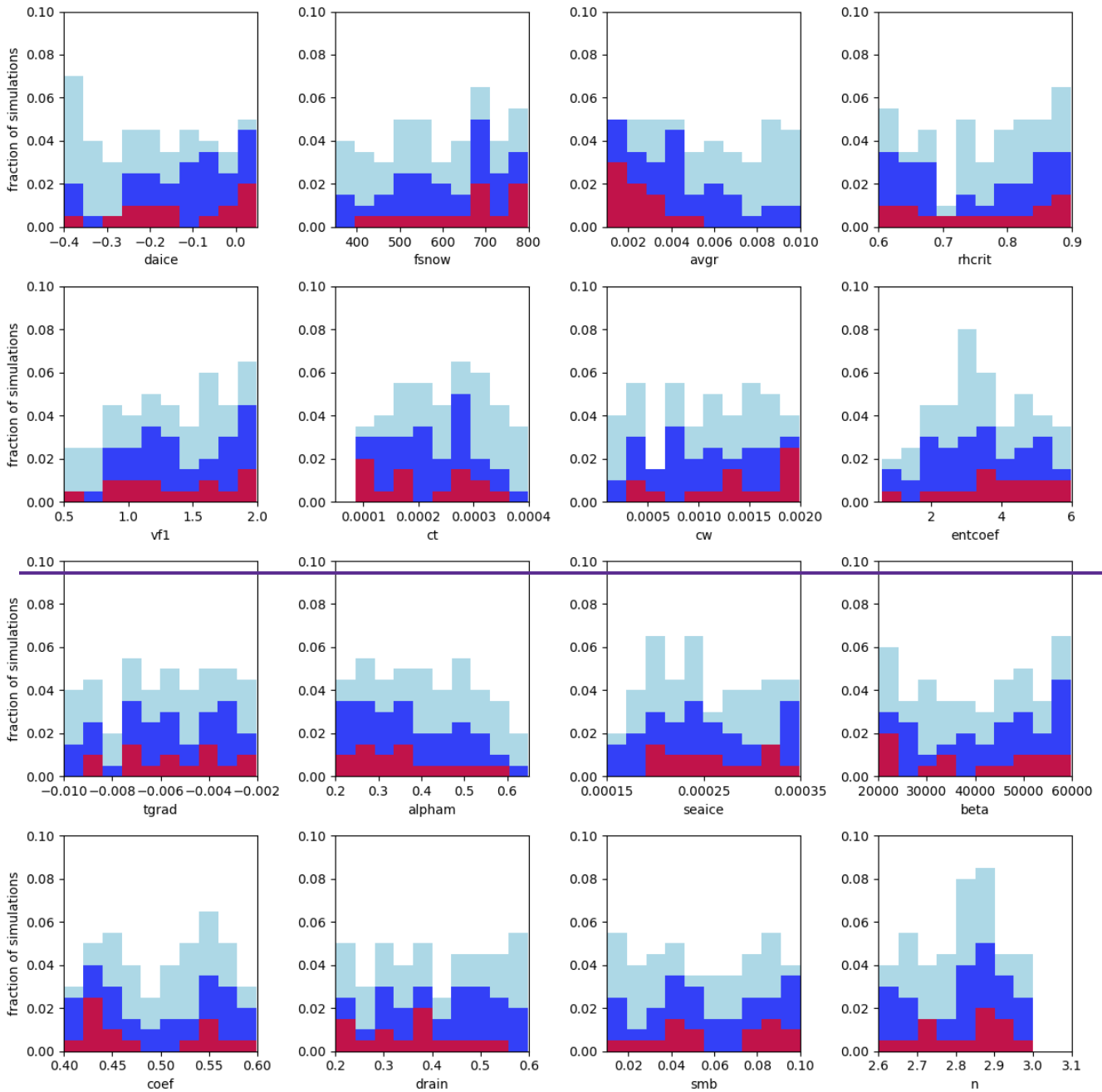
272
 273 Table 1 Summary of parameters modified in the ensemble simulations. ND stands for non-dimensional.

Name	Min value	Max value	Unit	Note
daice	-0.4	0.05	K^{-1}	Darkening effect of warm surface air temperature on bare ice in the albedo scheme, mimicking water collecting at the surface. Minimum value reduces the bare ice albedo to as low as 0.15 (Smith et al. 2021).
fsnow	350	799	$kg\ m^{-3}$	Density threshold for snow in the albedo scheme beyond which the surface starts to be regarded as bare ice. Higher values correspond to using brighter albedoes for denser snow and tends to increase ice sheet albedo (Smith et al. 2021).
avgr	0.001	0.01	μm^{-3}	Dependence of snow albedo on increasing grain size. Higher value enhances the darkening of snow over time and reduces the snow albedo (Smith et al. 2021).
rhcrit	0.6	0.9	ND	Threshold of relative humidity to form large-scale clouds (Smith, 1990).
Vfl	0.5	2.0	$m\ s^{-1}$	Speed of ice sedimentation (Heymsfield, 1977).
ct	0.00005	0.0004	s^{-1}	Conversion rate of cloud liquid water droplets to precipitation (Smith, 1990)
cw	0.0001	0.002	$kg\ m^{-3}$	Threshold value of cloud liquid water for formation of precipitation (Smith, 1990). Only values over land are modified.
entcoef	0.6	6.0	ND	Entrainment rate coefficient. Higher value enhances mixing of an ascending convective plume with ambient dry air.
tgrad	-0.01	-0.002	$K\ m^{-1}$	Air temperature lapse rate used during the downscaling to ice sheet surfaces. Larger negative values correspond to stronger lapse rate effects (Smith et al. 2021).
alpham	0.2	0.65	ND	The lowest value of albedo in the sea ice scheme.
seaice	0.00015	0.00035	$m^2\ s^{-1}$	Efficiency of heat exchange between the base of sea ice and ocean. Higher value increases the heat flux and causes a retreat of sea ice.
beta	20000	60000	$Pa\ m^{-1/3} a^{1/3}$	Coefficient in Weertman-friction law. Higher value corresponds to stronger friction between the ice base and the dry bedrock (Gandy et al. 2019).

coef	0.4	0.6	ND	Coefficient in Coulomb-friction law (Gandy et al. 2019).
drain	0.2	0.6	$m yr^{-1}$	Magnitude of drainage removing water from the till. Higher value removes water rapidly from the till hence increases the Coulomb-friction (Gandy et al. 2019).
smb	0.01	0.1	$m yr^{-1}$	Magnitude of temporally constant and spatially uniform surface mass balance (expressed as equivalent liquid water volume flux) applied during the standalone BISICLES spin-up. Higher values result in a larger ice sheet at the beginning of the FAMOUS-BISICLES coupled simulation.
n	2.6	3.1	ND	Coefficient in Glen's flow law.

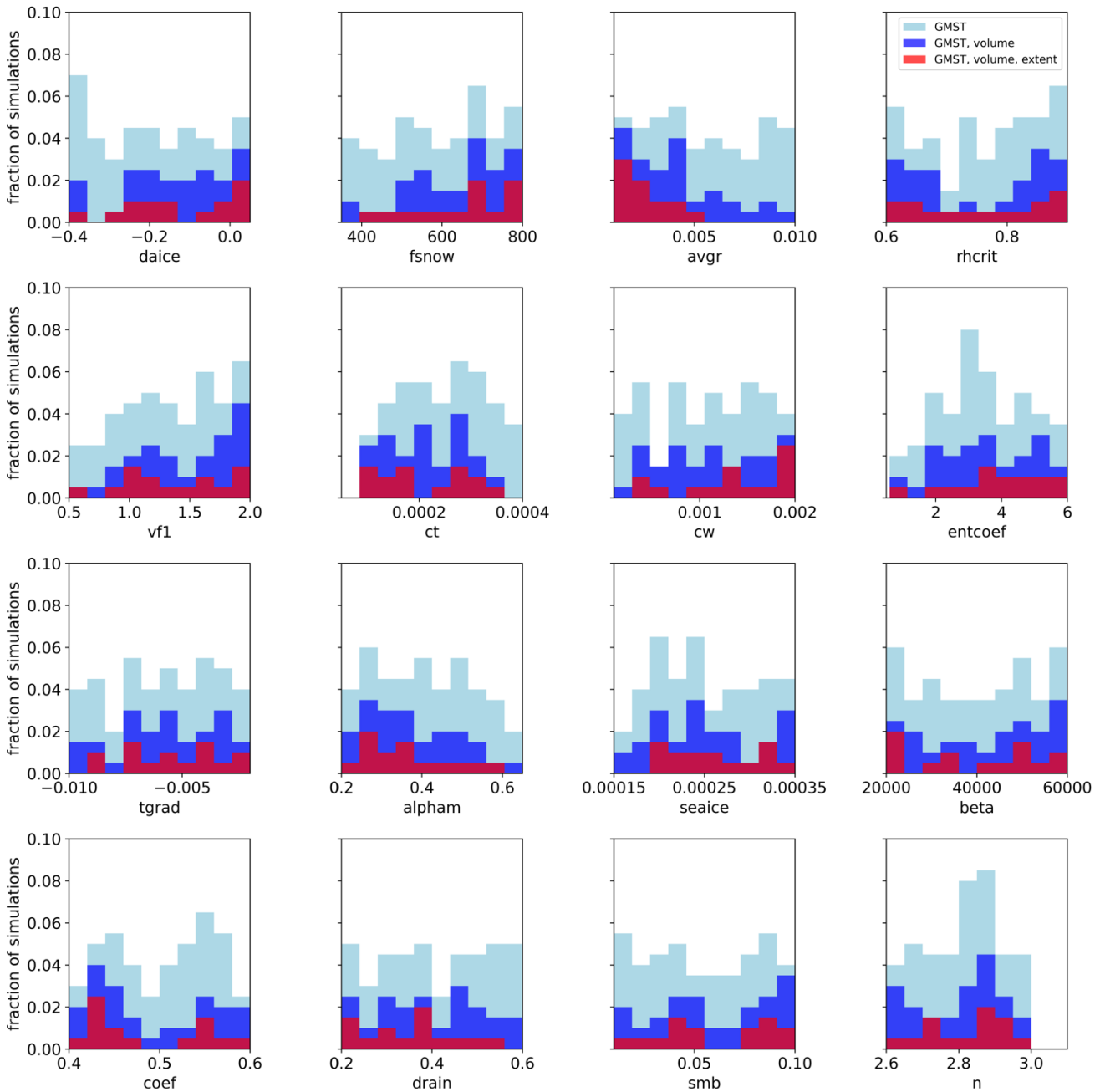
274

275



276

277



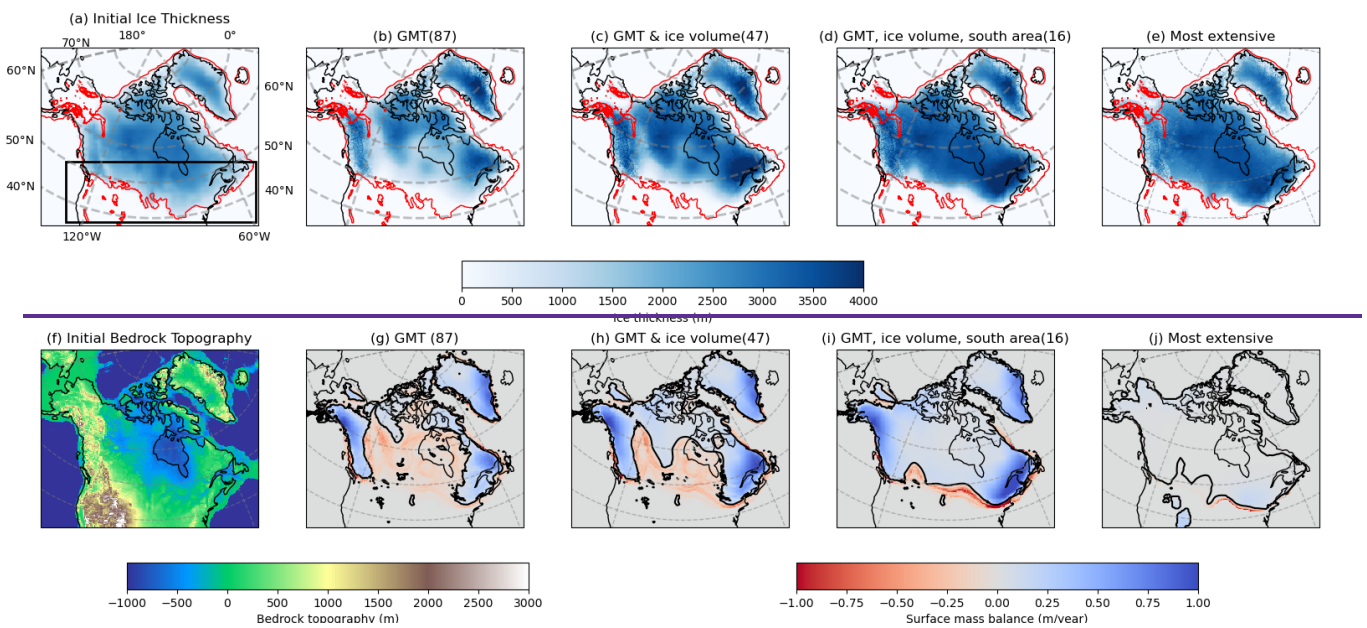
278

279 Fig. 2 Fraction of the 200 simulations which satisfy the constraints as a function of each of the parameters. 200 members are
 280 uniformly distributed in each parameter range based on the latin-hypercube sampling method (approximately 20 simulations
 281 per each parameter bin). Light blue: ensemble members satisfying the global [mean surface temperature \(GMST\)](#) constraint,
 282 Dark blue: ensemble members satisfying [both the global temperature GMST and total the North American](#) ice volume
 283 constraints, Red: ensemble members satisfying [the southern North American ice sheet margin](#) constraints in addition to
 284 [global temperature the GMST and total the North American](#) ice volume constraints.

285 **2.3 Integration procedure**

286 Model simulations are all initiated from a static, isothermal (ice temperature 253 K) ice sheet and bedrock topography of
 287 21ka BP of GLAC-1D (Fig. 3a, f, Tarasov et al. 2012). The simulations have two phases. First, there is an initial [spin-up of](#)
 288 5000 ice sheet [year spin-up years](#) with stand-alone BISICLES, where the ice sheet model parameter values are chosen
 289 according to the ensemble Latin Hypercube sampling, but the associated climate parameter values are not used because there
 290 is no climate model. In place of the climate model, a constant-in-time surface mass balance (*smb*, Table 1) and atmospheric

291 surface temperature of 253K are applied uniformly over the ice. Note that the ice temperature is allowed to evolve in the
 292 simulation. The *smb* value is varied across the ensemble to produce a variety of total ice volumes (Fig. S1), because total ice
 293 volume is highly uncertain in reconstructions and could be important given the dependence of ice sheet simulation on initial
 294 conditions (Abe-Ouchi et al. 2013). The spin-up phase also gives the ice sheet model physics time to adjust from the
 295 prescribed initial condition, i.e. it allows BISICLES to smooth out the blocky surface of the ice sheet reconstruction,
 296 providing some stability to the simulations when they are subsequently coupled to the climate (FAMOUS) in the second
 297 phase. By the end of the spin-up phase, 200 unique ice sheets have been modelled, providing the starting condition for
 298 simulations with BISICLES coupled to FAMOUS in the second phase. In FAMOUS-BISICLES, *smb* is redundant and the
 299 climate parameters chosen by Latin Hypercube are used in FAMOUS, with the same ice sheet parameter combinations as in
 300 the spin-up phase. In the second phase, the simulations run ~~another~~for 5000 ice sheet (500 climate) years, which is
 301 insufficient to reach a quasi-equilibrium state, but sufficiently long to see the effects of important parameters on the climate
 302 and ice sheets. For some of the best-performing simulations, the integration is extended for another 5000 ice years-
 303 However, during which the configuration of the ice sheet showedshows only modest further changes (Fig. S2).



304
 305

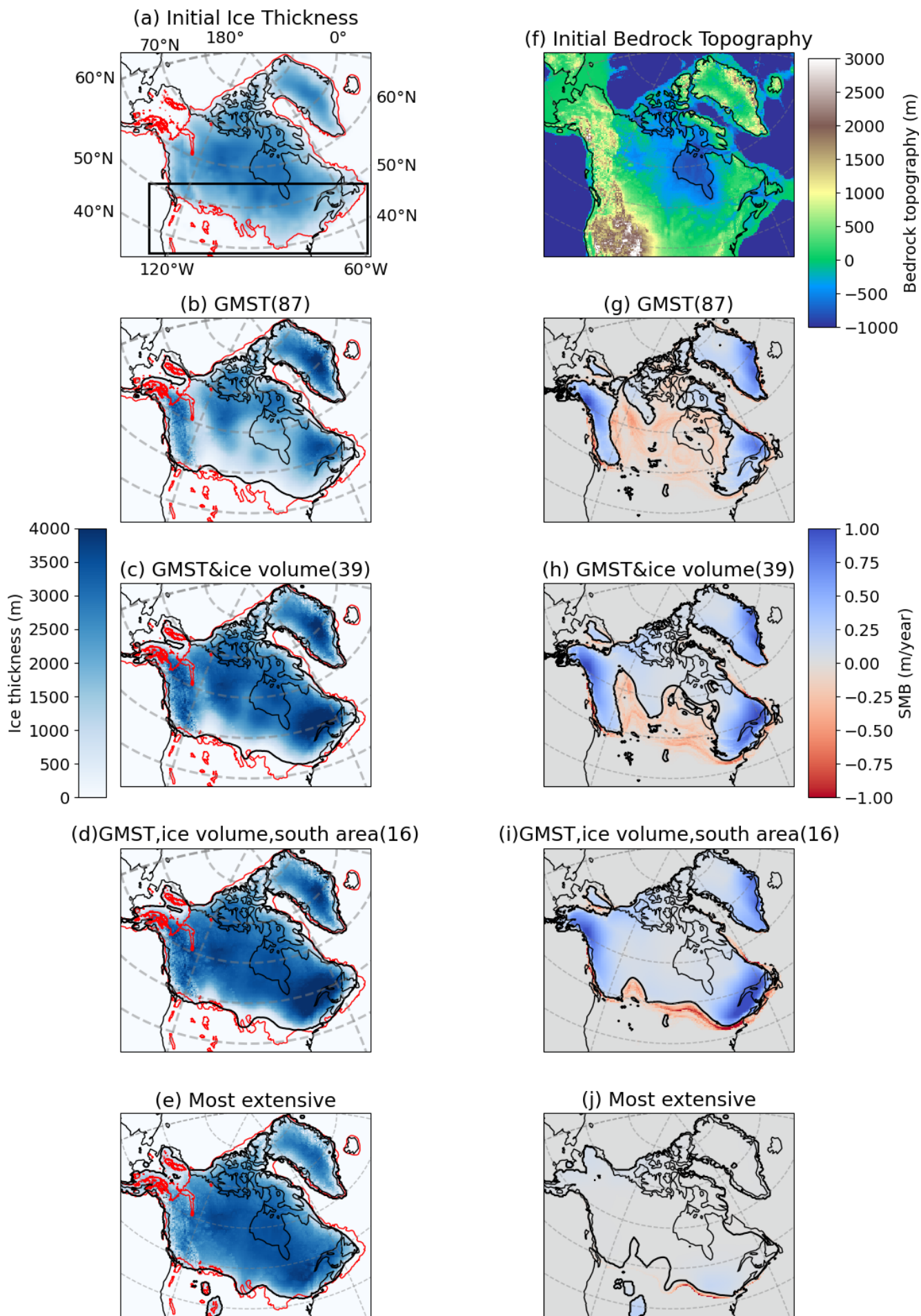


Fig. 3 Spatial maps of the initial condition for the ice sheet model, and results from the FAMOUS-BISICLES ensemble after 5000 ice sheet years. (a) ice topography [m] and (f) bedrock topography [m] from Tarasov et al. (2012). (b-e/top) Spatial maps of ~~surface altitude~~ice thickness [m] and (g-j/bottom) surface mass balance (SMB) [m/year] from ensemble means. (b, g) 87 members satisfying the ~~global~~Global mean ~~surface~~ temperature (GMST) constraint, (c, h) 4739 members satisfying both ~~global mean temperature~~GMST and ice volume constraints, (d, i) 16 members having the largest southern extent of North American ice sheet that satisfies ~~temperature~~GMST and volume constraints and (e, j) the member with most extensive southern ice area in the ensemble simulations. The thin black contour corresponds to the modern coastline, whereas the thick black contour in (g-j) corresponds to the zero line of SMB. Red contours in (a)-(e) correspond to the ice extent of Dalton et al. (2020). Black contours in (b)-(e) correspond to the ice extent of the ensemble mean defined as 100 m ice thickness. Black rectangle in (a) shows the region where the southern extent of the North American ice sheet is calculated (e.g. Fig. 11).

2.4 Constraints

Three metrics are used to evaluate the large-scale feature of the ensemble simulations. These are the annual mean LGM ~~global surface air temperature, total~~GMST, the ice volume of the North American ~~and Greenland~~ice sheets~~sheet~~ and the southern extent of the North American ice sheet.

For the global temperature, we create our LGM constraint by adding estimates of the LGM global cooling to the Preindustrial ~~global temperature. The Preindustrial temperature is~~GMST of 13.7 °C (1880-1900, NOAA National Centers for Environmental Information (2023)) with an uncertainty of $\pm 0.1^\circ\text{C}$ (one standard deviation of global temperature during this period). According to previous studies, the LGM global cooling relative to the Preindustrial has a range of -1.7°C to -8.3°C (e.g., -1.7°C to -3.7°C with a probability of 90% in Schmittner et al. (2011) and -4.6°C to -8.3°C with a probability of 90% in Holden et al. (2010), see Fig. 4a in Tierney et al. 2020). To objectively cover all the possibilities, we take into account all of these studies to define our range of plausible LGM GMST. Assuming the LGM cooling is normally distributed, this gives a mean cooling of $5^\circ\text{C} \pm 3.3^\circ\text{C}$ with a probability of 90% (one standard deviation is $\pm 2.0^\circ\text{C}$). Combining the uncertainties associated with the Preindustrial ~~global temperature~~GMST and the LGM global cooling gives one standard deviation of the uncertainty of

$$\sqrt{(0.1)^2 + (2.0)^2} = \pm 2.0^\circ\text{C}$$

in the actual LGM ~~temperature~~GMST (66% probability). To be conservative and take into account model uncertainty, we apply three standard deviations ($\pm 6.0^\circ\text{C}$) as the uncertainty ranges. This gives an actual LGM ~~temperature~~GMST of approximately 2.7°C to 14.7°C ($8.7^\circ\text{C} \pm 6.0^\circ\text{C}$), with a probability of- at least 99% (Pukelsheim 1994).

For the ~~total~~ ice volume constraint, previous studies have suggested that the volume of the North American ice sheet was likely to be ~~higher~~larger than 6070 m sea level equivalent (c.f. Abe-Ouchi et al. 2015). To account for model uncertainty and to be conservative, we apply a minimum reasonable North American ice volume of ~~50 m SLE as a constraint. 60 m SLE as a constraint. Applying an upper ice volume limit may also be important in constraining the parameter space. However, in general, equilibrium LGM simulations tend to overestimate the ice volume if once the simulation has a net positive SMB (e.g. Alder and Hostetler 2019). In this regard, setting an upper limit can be tricky, and therefore needs to be examined in a different experimental set-up.~~

The southern extent of the North American ice sheet is used to select the best-performing simulations, rather than as a strict constraint, because all ensemble members show a smaller southern area of the ice sheet than reconstructions (see Section 4.1). Areas of grid cells covered by the ice sheet in the box shown in Fig. 3a are calculated. This area corresponds to the

348 [south of the Hudson Bay](#). Simulations with the southern area covering 60% of the ~~reconstruction~~[reconstructed area](#) (Dalton
349 et al. 2020) are considered to satisfy our constraint.

350

351 In the end, sixteen simulations simultaneously satisfy our constraints on temperature, ice volume and extent.

352 3. Results

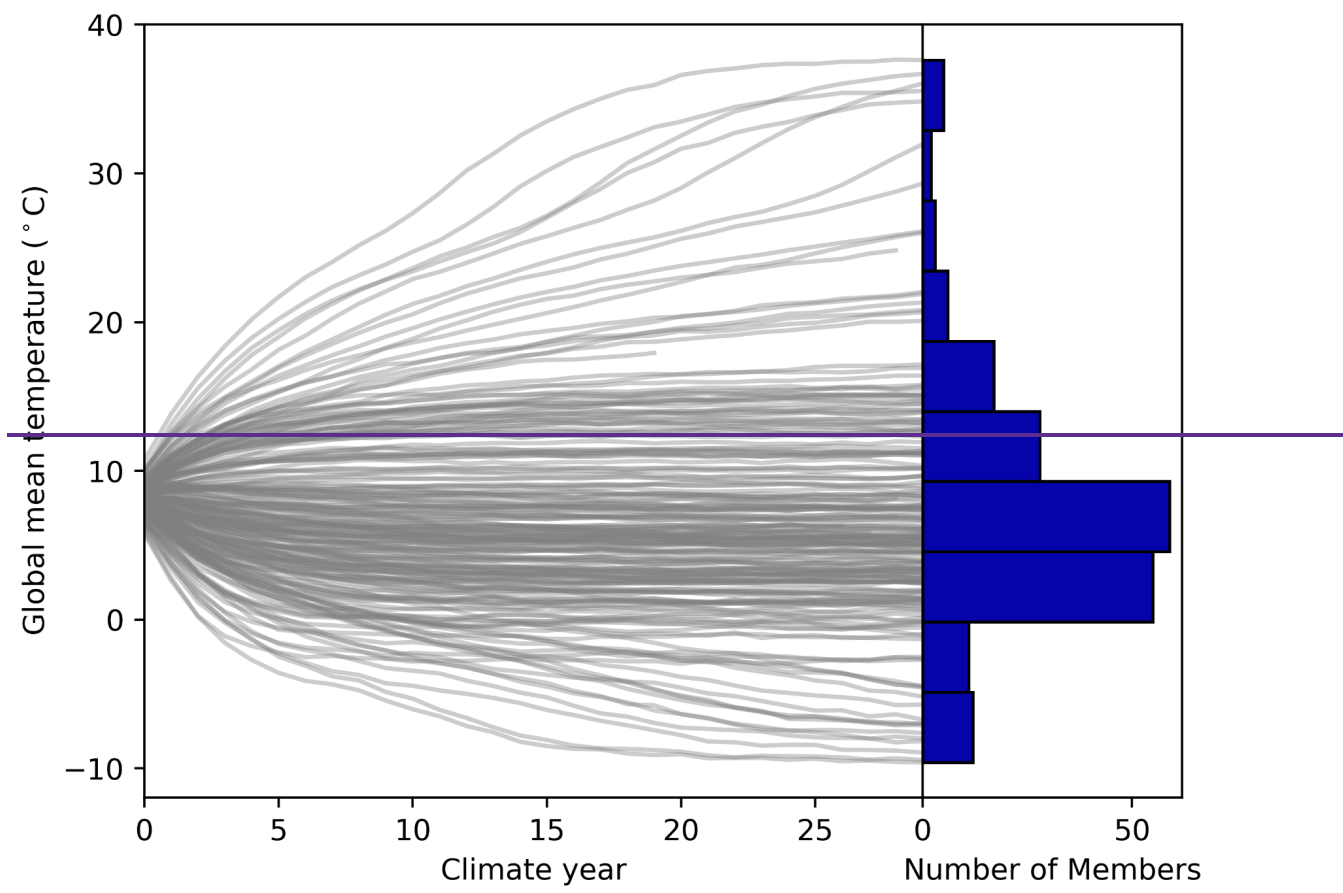
353 3.1 Response of the [Global temperature GMST](#)

354 Fig. 4 summarises the temporal evolution of annual mean ~~global mean temperature~~[GMST](#) in the ensemble of simulations.
355 After the first 300 ice sheet years, climates reach a quasi-equilibrium. The results show a wide variety of simulated global
356 temperatures, ranging from -10°C to 40°C . Such a wide range is frequently observed under parameter ensemble simulations
357 (e.g. Joshi et al. 2010, Gregoire et al. 2011). The diverse response of [global temperature GMST](#) is largely explained by two
358 parameters in the cloud schemes; ct in the large-scale condensation scheme and $entcoef$ in the cumulus convection scheme
359 (Fig. 5). The correlation coefficients of these parameters with the global temperature at ice years 200-290 are 0.622 for ct
360 and -0.574 for $entcoef$, respectively. In contrast, other parameters appear to have a smaller effect, according to the correlation
361 analysis (Fig. 5). For the sea ice albedo, this relatively muted sensitivity may be related to the use of a slab ocean model,
362 which underestimates the strong interactions between sea ice and oceanic heat transport over the Southern Ocean that
363 amplifies the surface cooling at high latitudes (Ogura et al. 2004, Zhu et al. 2021). Including a dynamical ocean may increase
364 the importance of sea ice albedo on the [global temperature GMST](#), as shown by Gregoire et al. (2011).

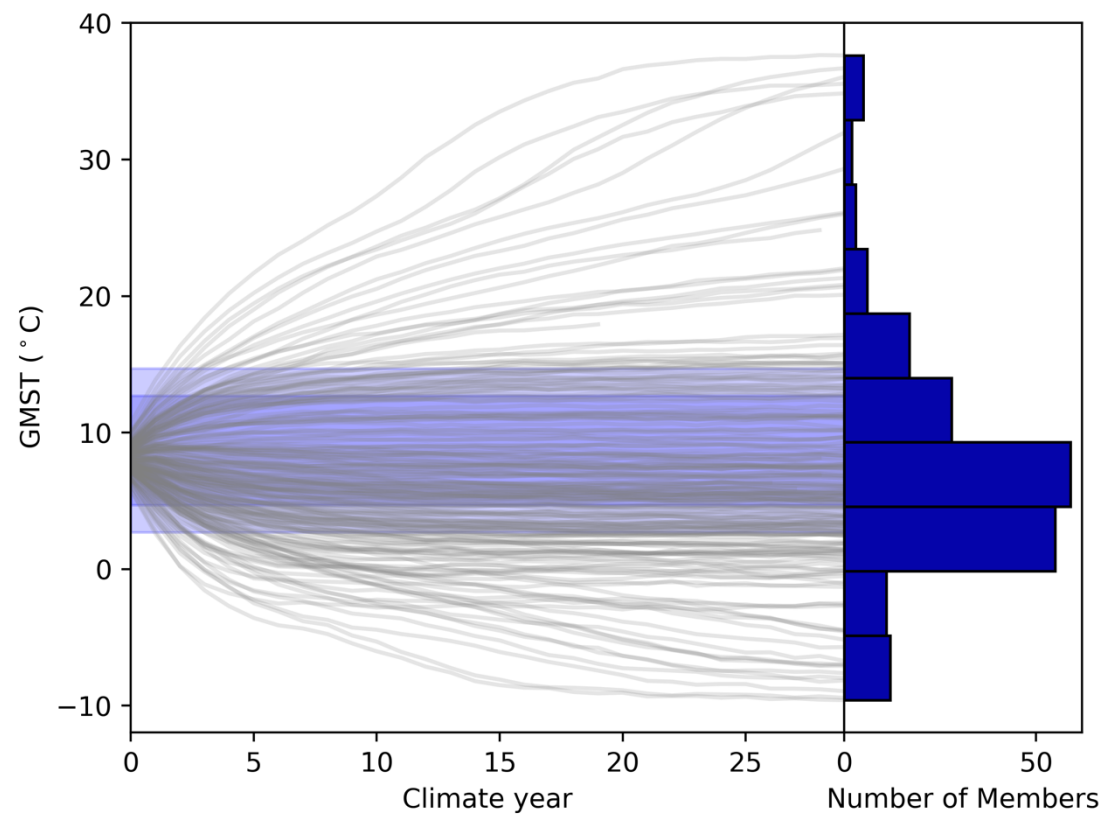
365

366 Roles of ct and $entcoef$ in governing [global temperature GMST](#) are further explored by means of a pair plot in Fig. 6. This
367 figure compares the relationship of these two parameters to ~~global temperature~~[GMST](#). The results show a positive
368 correlation between global-scale warming and ct , which is associated with an increase in precipitation efficiency, reducing
369 the life cycle of mid-latitude clouds, causing a decrease in the cloud cover and a decrease in the planetary albedo. As a result,
370 more shortwave radiation is absorbed and the planet warms (Joshi et al. 2010, Sherriff-Tadano et al. 2023). Conversely,
371 global-scale warming occurs with decreasing $entcoef$ (Fig. 6), as the entrainment rate of ambient dry air in the tropics
372 reduces, and the vertical transport of moisture to the high troposphere and lower stratosphere enhances. The planet then
373 warms up due to the strong greenhouse gas effect of the water vapour (Joshi et al. 2010). Similar responses are observed in
374 Joshi et al. (2010), who performed ensemble simulations under modern and future climates and showed that low values of
375 $entcoef$ were unrealistic based on the amount of water vapour in the lower stratosphere. Consistently, ensemble members
376 with very low values of $entcoef$ are more likely to be ruled out for producing implausible ~~global mean temperatures~~[GMSTs](#),
377 depending on the effect of the combinations of the other parameters (Fig. 6). For ensemble members satisfying the
378 temperature constraint (black outlined coloured dots in Fig. 6), the overall cooling and warming effects of ct and $entcoef$ are
379 largely cancelled out by each other.

380

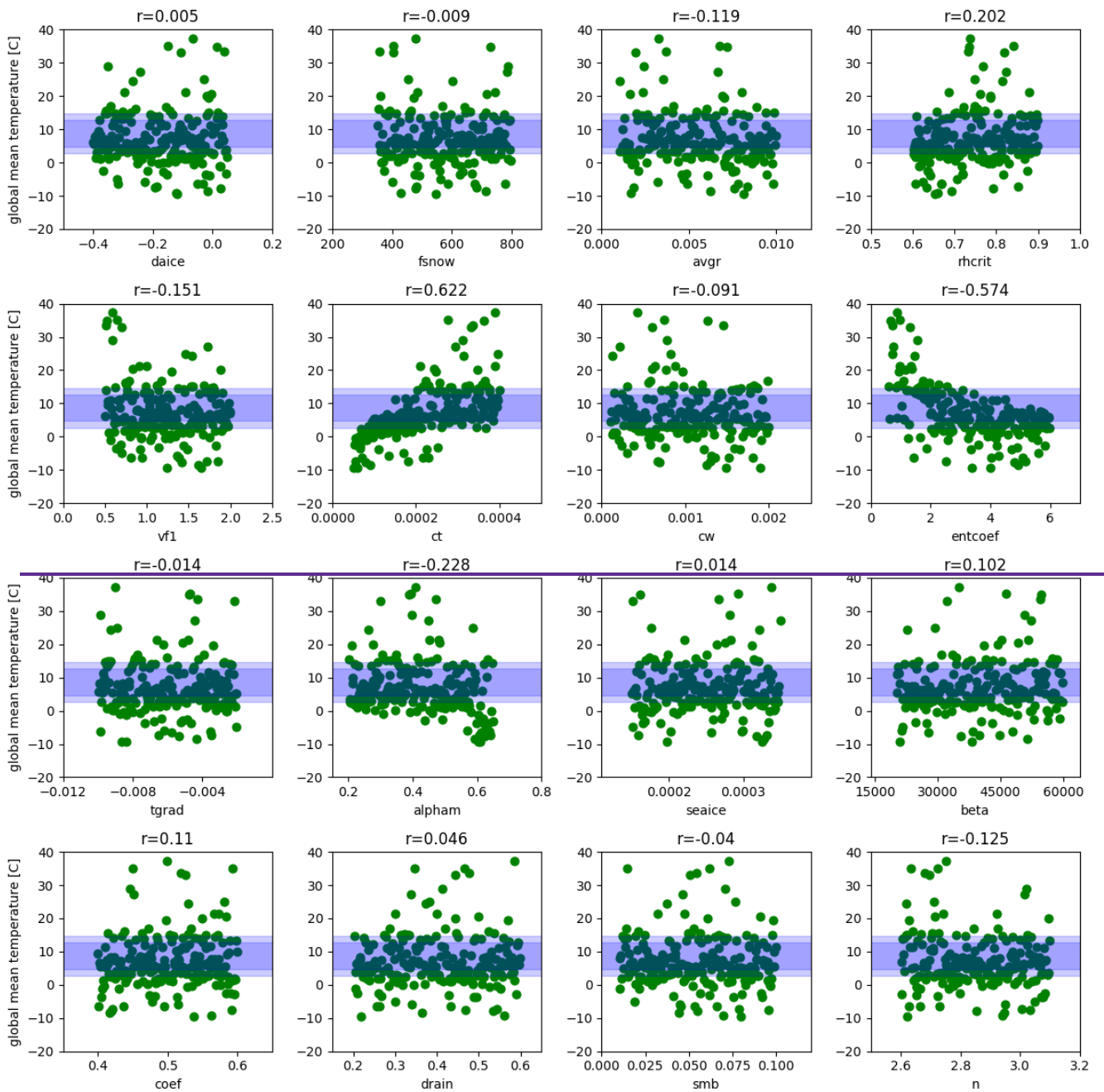


381
382

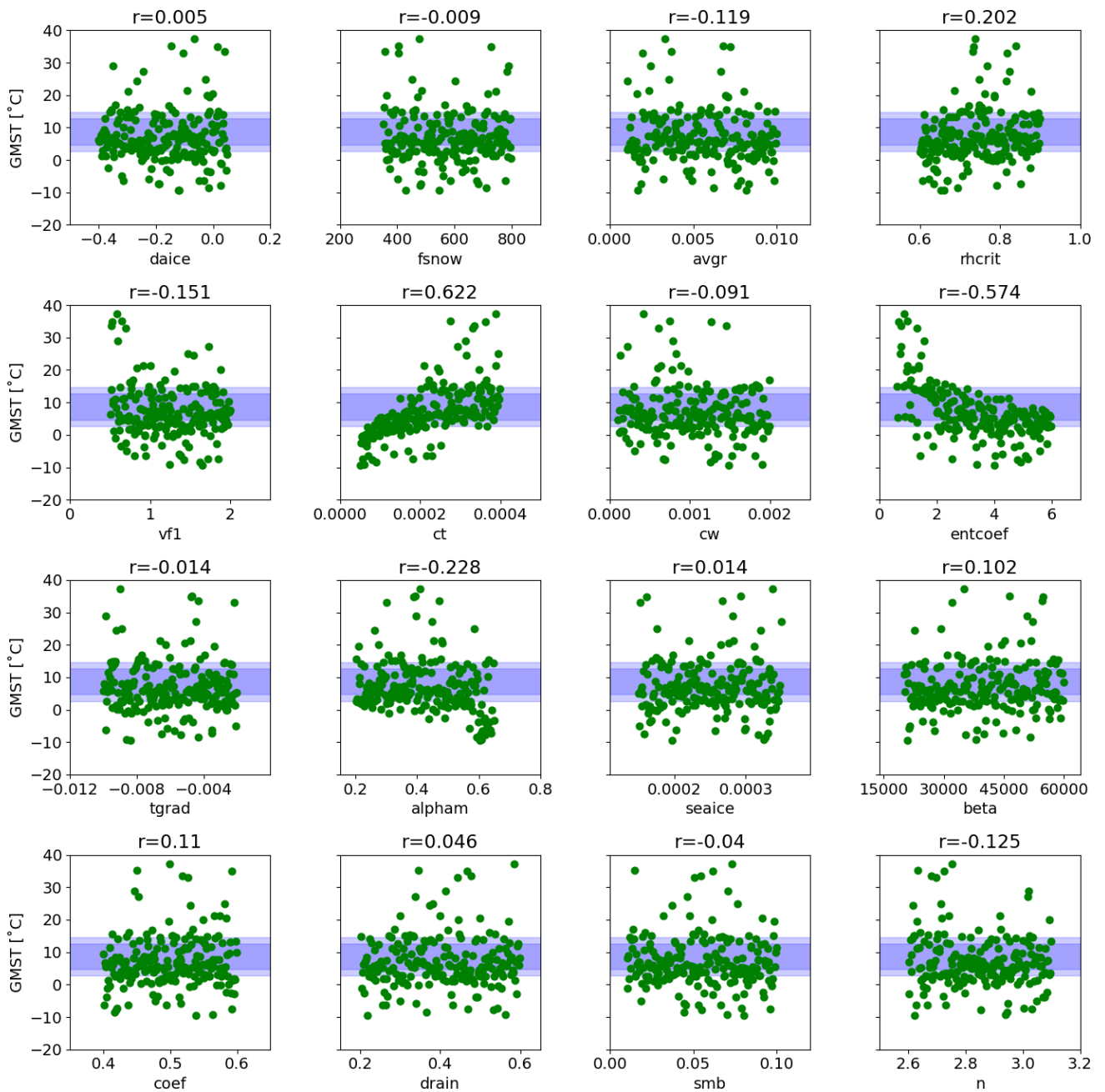


383

384 Fig. 4 Evolution of global mean annual temperatureGMST in the Famous-BisiclesFAMOUS-BISICLES ensemble of
 385 simulations. Each grey line represents one ensemble member. Results from the first 300 ice years (30 climate years) are
 386 shown. The uncertainties in GMST are shaded blue (three standard deviations for light blue and two standard deviations for
 387 dark blue). Histograms on the right show the number of simulations in each temperature bin.



390
391



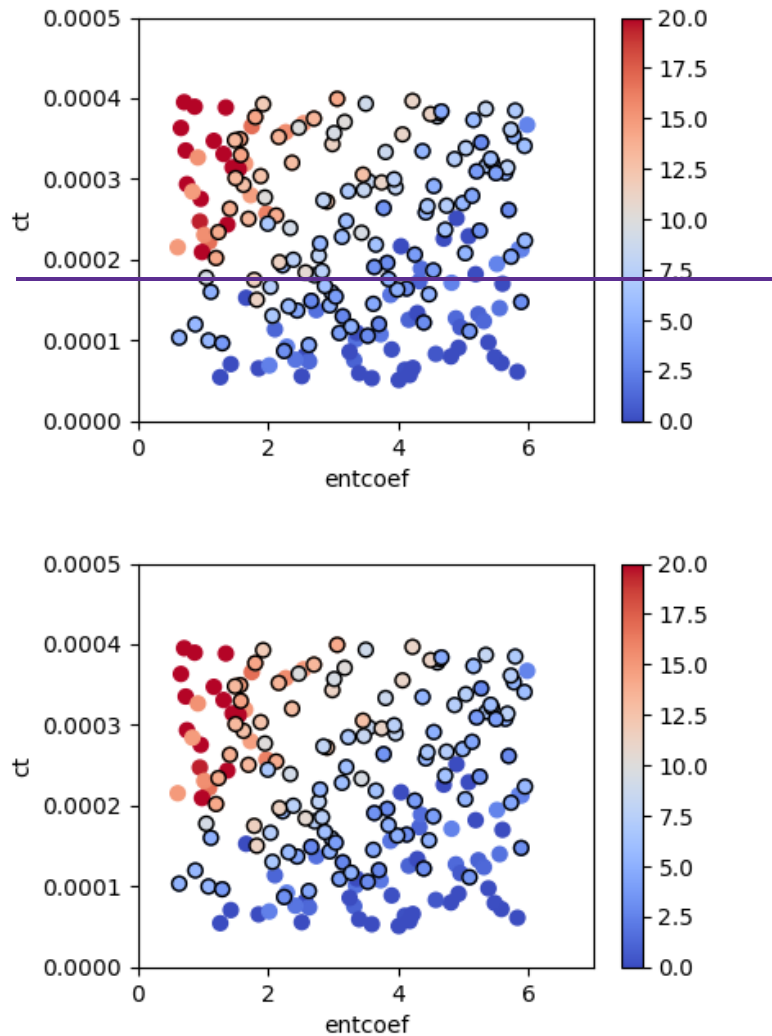
392

393 Fig. 5 Relationship between [global mean temperature GMST](#) averaged over ice years 200-290 (climate years 20-29) and each

394 parameter value. Correlation values are displayed above each panel. The uncertainties in [global mean annual surface air](#)

395 [temperature GMST](#) is shaded blue (three standard deviations for light blue and two standard deviations for dark blue).

396



397

398

399

400

401

402

403

404

405

406

407

408

409

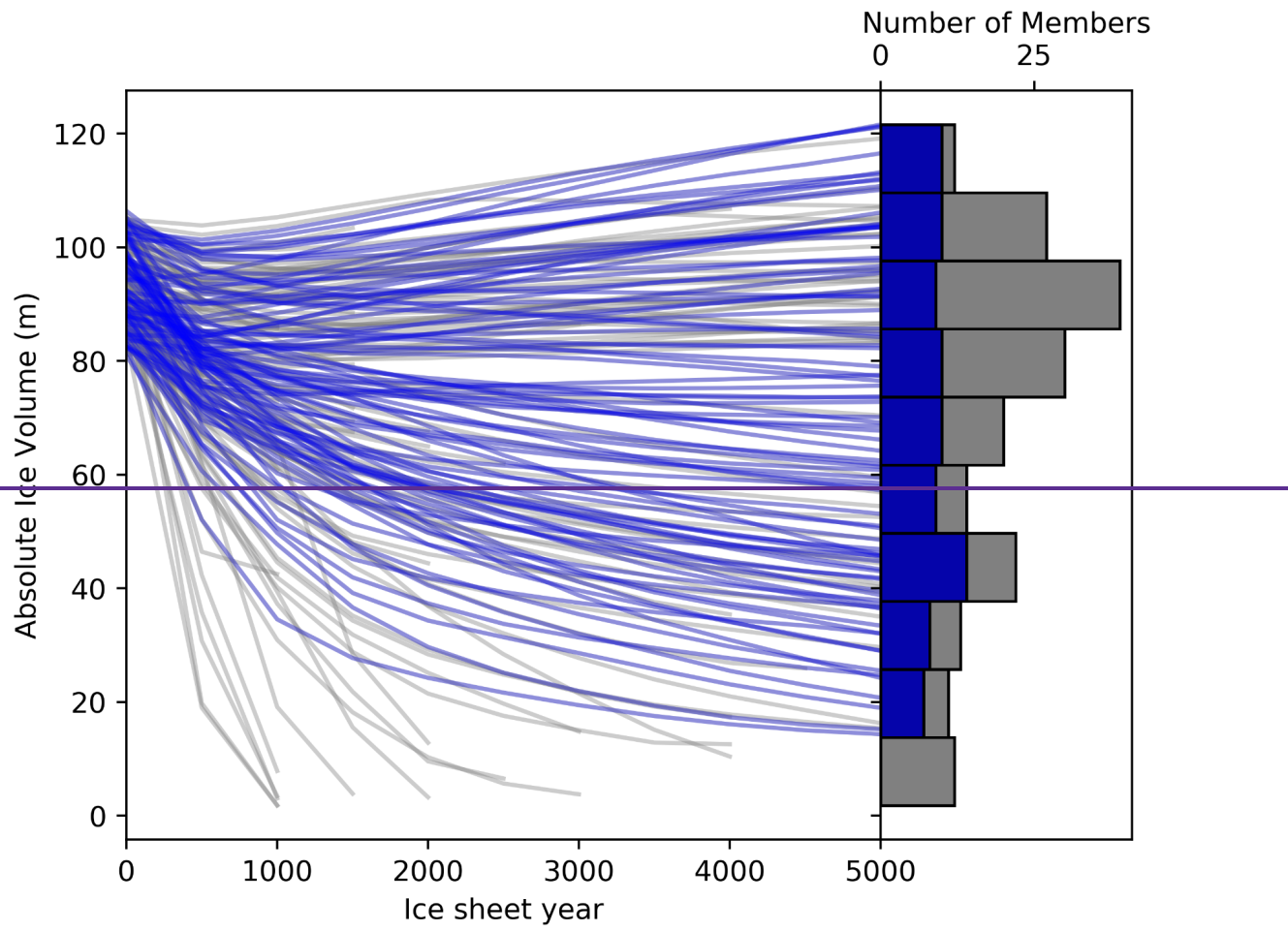
410

411

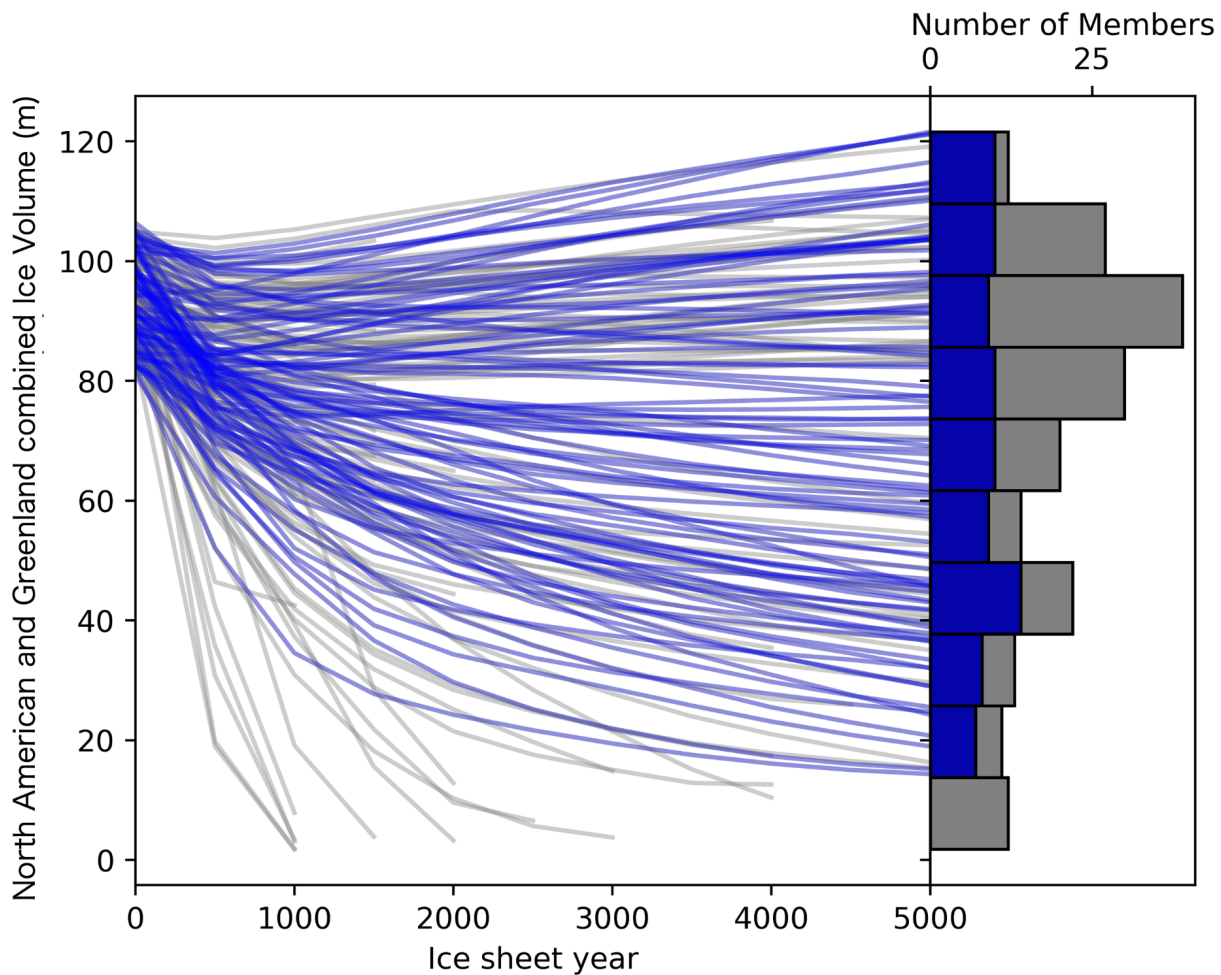
Fig. 6 Pair plot analysis exploring the combined effects of ct (precipitation efficiency in the large-scale condensation scheme) and $entcoef$ (entrainment rate in the cumulus convection scheme) on [global mean annual surface air temperature GMST](#) (colours, °C). Filled circles outlined in black are those satisfying the temperature evaluation criterion.

3.2 Response of the North American ice sheet ~~and absolute ice volume~~

Similar to the diversity in simulated [global mean temperature GMST](#), the evolution of the ice sheet after the coupling to FAMOUS shows a wide range of responses (Fig. 7). Starting from [absolute combined](#) ice sheet volumes of 80 to 105 m SLE (sum of North American and Greenland ice sheets), the ensemble members produce [absolute combined](#) ice volumes between 0 and 120 m SLE at the end of the 5000-ice year integration. In some simulations, even the Greenland ice sheet disappears completely associated with the very high global temperature (Fig. 4). Note that some simulations with high n values or very warm climates (that cause all of the ice to rapidly disappear) crash during the integration. In total, 139 members (~ 70% of the ensemble) complete the entire 5000 ice years. Eighty-seven members satisfy the global temperature constraint (Fig. 5 and Fig. 6) , and [4739](#) members also satisfy the North American ice volume constraint of at least [5060](#) m SLE. The additional constraint on the southern extent of the North American ice sheet selects the 16 best performing simulations (Fig. 2).



412



413
 414 Fig.7 Evolution of absolute ice volume of the North America and Greenland combined SLE ice volume in the
 415 FAMOUS-BISICLES LGM ensemble. Note that the modern ice volume of the entire 7.3 m SLE on Greenland is included;
 416 the ice volume is not the difference between LGM and present. Each grey line represents one ensemble member. Blue lines
 417 are the members satisfying our chosen global temperature GMST evaluation criteria. Histograms on the right show the
 418 number of simulations in each temperature bin; grey: all members and blue: members satisfying the global
 419 temperature GMST constraint.

420
 421 To explore which parameters are causing the variety of outcomes for the simulated North American ice volume, scatter plot
 422 and correlation analyses are performed (Fig. 8). Here, the ensemble members that both satisfy the global temperature GMST
 423 constraint and have completed 5000 ice years are used (87 members). The analysis shows important impacts from
 424 parameters in our ice sheet surface albedo scheme that have a direct influence on the albedo that is diagnosed for bare ice or
 425 uncompacted snow surfaces; *avgr* (snow ageing effect), *daice* (melt pond effect), and *fsnow* (the weighting of snow and ice
 426 albedo based on the density of snow) showing correlations of -0.56, -0.475 and 0.372, respectively, with ice volume (see
 427 Table 1 for the effects of each parameter). Similar results are obtained for the analysis on the southern extent of the North
 428 American ice sheet (Fig. S4).

429
 430 Additional analysis exploring the combined effect of these three parameters in the albedo scheme reveals a strong
 431 dependence between *daice* and *fsnow* (Fig. S7); the ice volume is less sensitive to *daice* when *fsnow* has a large value. This
 432 is reasonable as a large value of *fsnow* means that most of the snow/ice will be diagnosed as snow due to the high value of
 433 density threshold. As a result, the darkening effect for the old ice (*daice*) has only a minor influence.

434

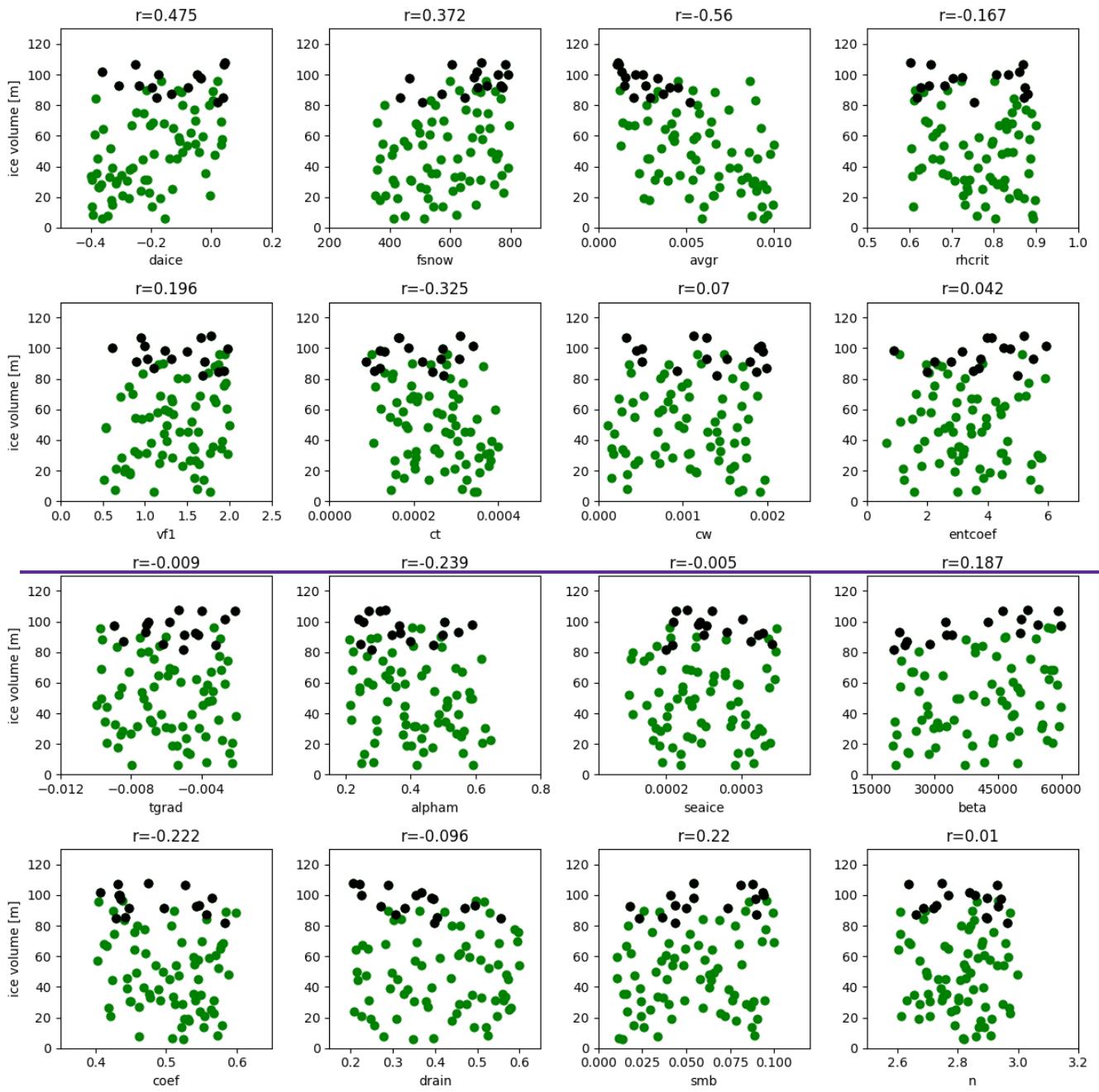
435 The effects of other climate parameters are weaker compared to those of albedo parameters. Among these, ct shows the
436 largest correlation value of -0.325. This is reasonable since the low value of ct corresponds to a colder global climate (Fig.
437 5), hence a colder local climate over the ice sheet, allowing the large ice sheet to be sustained (see also section 3.4 and Fig.
438 11). On the other hand, the 87 not-ruled-out-yet simulations are relatively insensitive to $entcoef$ (Fig. 8). This may in part be
439 due to the screening out effect of ensemble members with low values of $entcoef$ that causes drastically warm climates. We
440 should also note that the cloud parameters exert some local influences on accumulation patterns, e.g. over the Gulf stream
441 region (Fig. S6); larger values of ct and cw correspond to an increase in the amount of snowfall in this area. However the
442 overall low correlation values between cw and the ice volume of North America shows a relatively weak effect of
443 accumulation on the simulated ice volume.

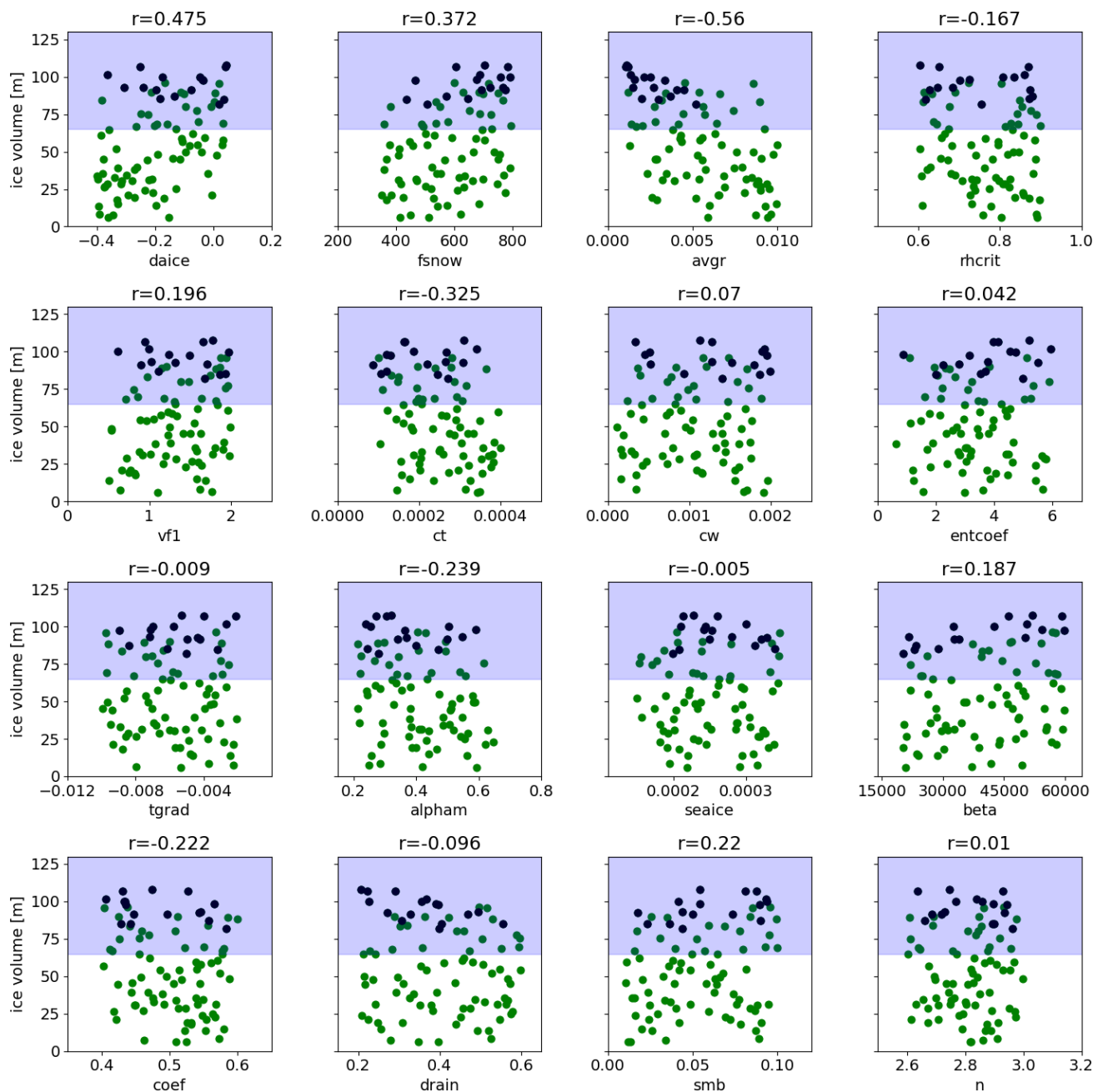
444

445 Correlation analysis shows a very weak effect from basal drag parameters ($beta$ and $coef$) on the ice volume (Fig. 8) and the
446 southern extent (Fig. S4). The correlation value of smb , which controls the initial ice volume when the coupled climate-ice
447 sheet phase of each simulation starts, is also low ($r=0.22$). This suggests only a weak connection between final ice sheet
448 volume at 5000 years and its initial volume at the beginning of the coupled simulations- [\(Similar results are also obtained for](#)
449 [ice volume changes in the first 500 years, Fig. S3\)](#). This is due to the large modifications in snow/ice albedo in our ensemble
450 design, which is capable of drastically altering the magnitude of absorbed solar radiation over the ice sheet (e.g. Abe-Ouchi
451 et al. 2013). For other dynamical ice sheet parameters ($drain$ and n), the correlations are generally even lower. Overall, the
452 North American ice sheet volume is much less sensitive to uncertainty in ice sheet dynamics than ice sheet albedo and
453 climate in our parameter space.

454

455 Interestingly, we find that the main results showing the importance of albedo parameters can be found in the first 500 ice
456 sheet years by analysing the relation of ice volume changes and each parameter (106 members, Fig. S3). Similar results are
457 also obtained by Gregory et al. (2020), who show that the SMB of the first 100 years can be a good predictor of the final
458 steady state ice sheet mass of modern and future Greenland. These results suggest that significant computational cost could
459 be saved for at least an initial exploration of model sensitivity to uncertain parameter values (e.g. if designing a multi-wave
460 ensemble experiment).





462

463 Fig. 8 Relationship between North American ice volume at 5000 ice years in FAMOUS-BISICLES and each perturbed
 464 parameter. Only those ensemble members that satisfy the [global temperature GMST](#) constraint are used. Correlation values
 465 are displayed above each panel. Black dots correspond to the best sixteen members. [The uncertainties in the North American](#)
 466 [ice volume constraint are shaded blue.](#)

467

468 To explore our preferred parameter space that produces good climate and ice sheets at the LGM, the distributions of
 469 parameters satisfying the applied constraints are examined (Fig. 2). Results show that some of the parameter ranges may be
 470 ruled out due to poor resulting simulation performance, such as values below 400 of *fsnow*, values above 0.006 of *avgr*,
 471 values below 0.00008 of *ct* and values above 3.0 of *n*. Additionally, from Fig. S7, a combination of low values in both *daice*
 472 and *fsnow* may be ruled out. Runs that satisfy the constraints tend to have parameters that lead to higher albedo values. For
 473 other parameters, it is shown that values across any individual parameter range in the ensemble can produce reasonable
 474 [global temperatures GMSTs](#) and ice sheets, depending on their combination with others.

475

476 The performance of the simulated ice extent in the best sixteen simulations (Fig. 3d) is further evaluated against the ice
477 extent reconstruction from Dalton et al. (2020, red contour in Fig. 3d). In general, the average of the best sixteen simulations
478 reproduces the overall ice extent of the North American ice sheet reasonably well; e.g. performances over the northern
479 margin and the southern margin west of 110°W and east of 80°W are reasonable. Also the performance is much better
480 compared to means of members that satisfies the global temperature GMST and the ice volume constraints but not the
481 southern North American ice margin criterion (Fig. 3b, c). In contrast, the main differences between the best sixteen
482 simulations and the reconstruction appear over the southern margin at 110°W - 80°W, where the model underestimates the
483 area of the ice sheet. Another difference can be found over Alaska, where the model overestimates the ice sheet area and
484 thickness (Fig. 3d). These features are commonly observed in ice sheet model simulations coupled to a low-resolution
485 atmospheric model and will be discussed in section 4.1.

486

487 Away from the southern margin, the best performing FAMOUS-BISICLES simulations tend to lack sufficient ice at the
488 eastern margin, where an ice shelf should exist (Fig. 3d). This is associated with the strong and uniform basal ice shelf
489 melting applied in this study. The basal melting around the coastal area largely depends on the configuration of the
490 continental shelf as well as the ambient ocean temperature, as shown by studies on the Antarctic ice sheet (e.g. Obase et al.
491 2017). Future work could undertake additional sensitivity experiments changing the magnitudes and patterns of the basal
492 melting to further explore this point.

493 3.3 Responses of the Greenland ice sheet

494 The Greenland ice sheet also shows various responses to modifications in the parameters in the ensemble of simulations,
495 ranging from 8 m SLE to 15 m SLE (Fig. 9). The simulated range is similar to the range in the reconstructions suggesting
496 9.3 m to 12.3 m SLE (7.3 m + 2~5 m SLE, Clark and Mix 2002, Lecavalier et al. 2014, Bradley et al. 2018, Tabone et al.
497 2018), while the model overestimates the higher band.

498

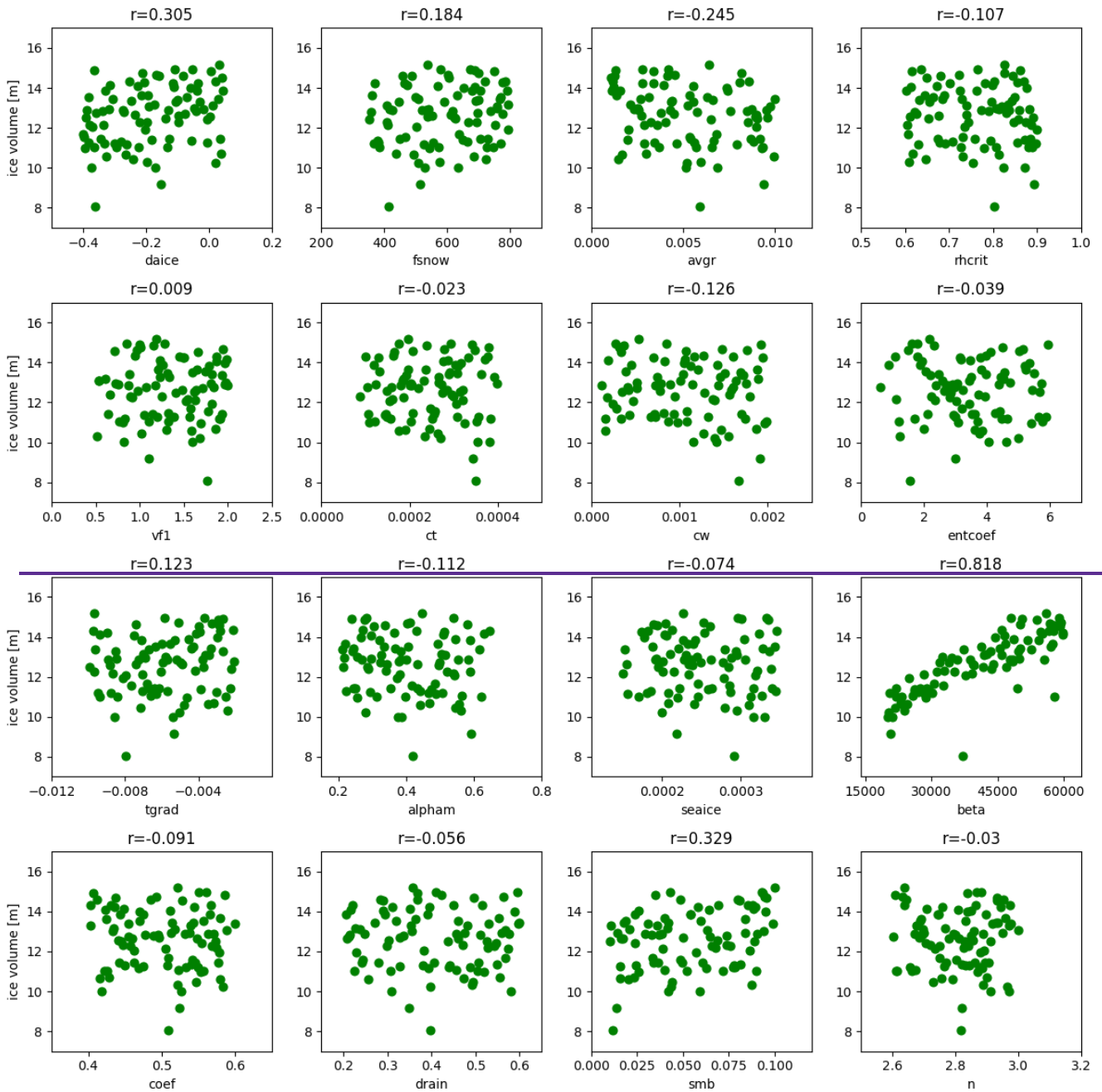
499 Interestingly, the results show a different sensitivity to the model parameters we vary compared to the North American ice
500 sheet (Fig. 9). The variations in the ice volume are mostly explained by changes in *beta*, where higher values increase the
501 friction between the ice sheet and the bedrock at a cold ice base. This acts to increase the ice volume by reducing the amount
502 of ice transported to its margin which then calves at the continental shelf, and hence by inducing thickening of the ice sheet
503 interior.

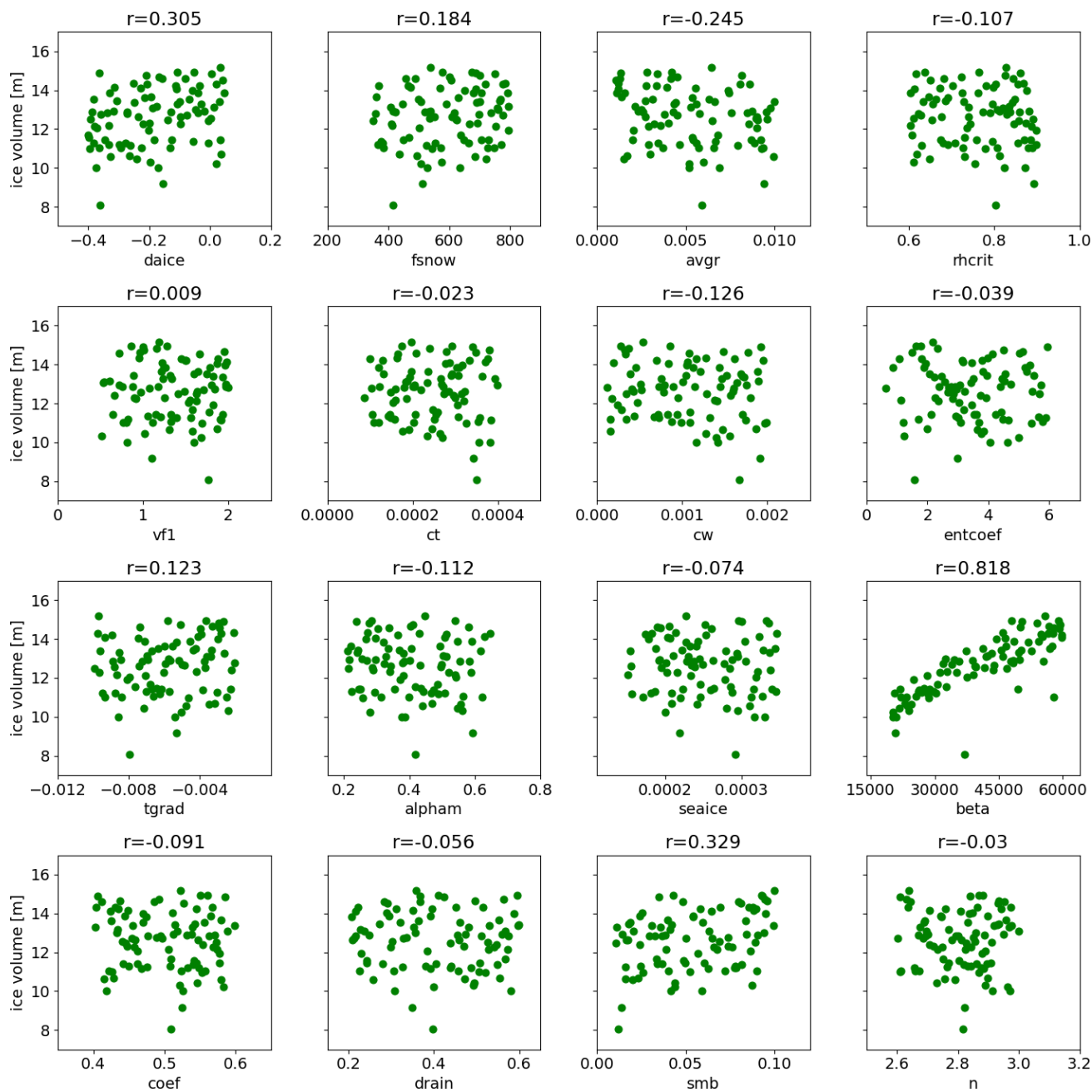
504

505 The lower sensitivity of the Greenland ice sheet to albedo parameters comes from different climatic conditions compared to
506 North America. In North America, the large area is covered by negative surface mass balance (Fig. 3g) as the summer
507 temperature can be close to freezing point in the simulations (Fig. 10). Hence, albedo parameters cause a drastic difference
508 since they control the magnitude of the negative SMB over North America (Fig. 8). In contrast, the Greenland ice sheet is
509 covered by colder conditions in summer (Fig. 10), hence most surface areas have positive surface mass balance (Fig. 9).
510 Under this condition, the amount of the ice loss is determined by the amount of ice transported from the interior to its edge,
511 which then calves. As a result, the ice volume is mainly driven by *beta* since it controls the transport of ice under the cold ice
512 base.

513

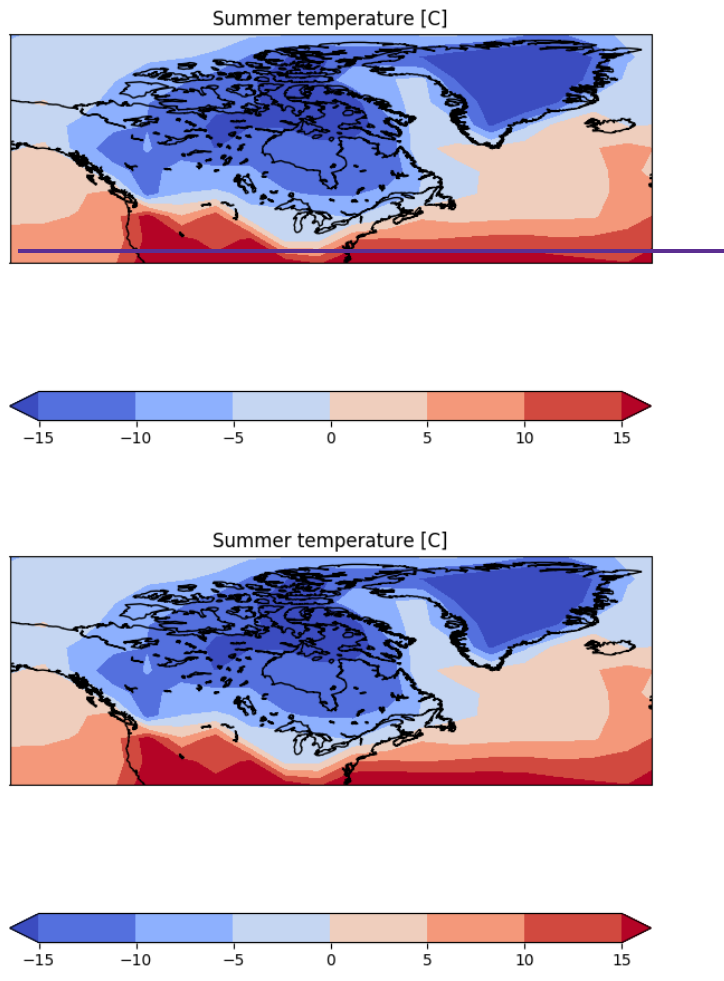
514 Previous studies have shown that basal melting of ice shelves by the underlying ocean is also important in controlling
515 Greenland ice sheet volume at the LGM in their coupled ice shelf-ice sheet models (Bradley et al. 2018, Tabone et al. 2018).
516 In this study, however, a constant value was given for the ice shelf basal melting. Conducting ensemble simulations with
517 variations in the amount of ice shelf melting may enable us to explore the relative importance.





521

522 Fig.9 Relation of ice volume of Greenland at 5000 ice years in FAMOUS-BISICLES and each parameter. Ensemble
 523 members satisfying the [global temperature GMST](#) constraint are used. Correlation values are displayed on the top of each
 524 panel.



525

526

527

528

529

530

531

532

533

534

535

536

537

538

539

540

541

542

543

544

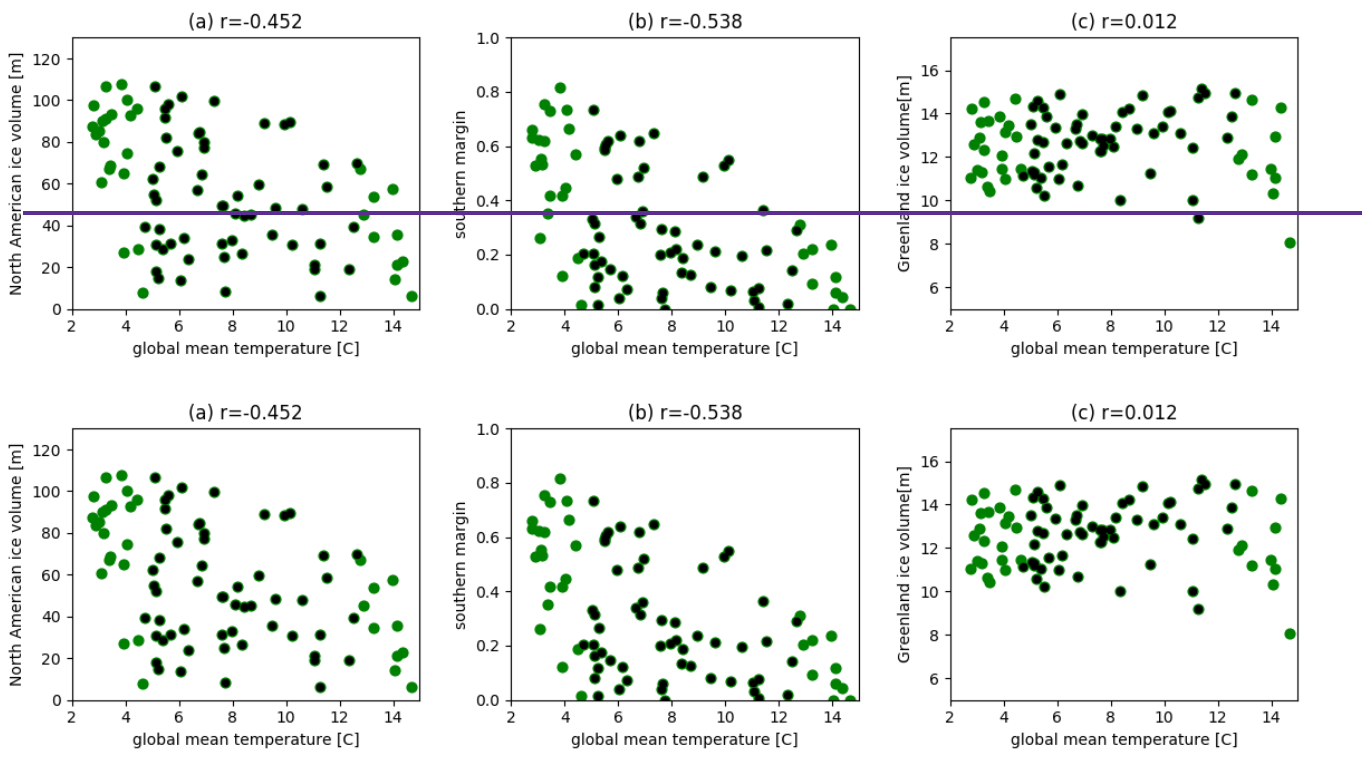
Fig.10 Summer surface air temperature [$^{\circ}\text{C}$] over North America and Greenland, averaged over all ensemble members satisfying the global temperatureGMST constraint.

3.4 Effects of global mean surface temperature (GMST) on ice sheet volume

The sensitivity of the ice sheets to the reasonable LGM global temperatureGMST range (2.7°C - 14.7°C) is explored to see any possible the relationship between them (Fig. 11). The results show a high correlation between the global temperatureGMST and North American ice volume/southern extent; colder climates correspond to larger and more extensive ice sheets (Fig. 11a, b). This is not a surprise since a large uncertainty of $\pm 6.0^{\circ}\text{C}$ is applied to the global temperatureGMST. Reducing the uncertainty level to two sigma ($8.7^{\circ}\text{C} \pm 4.0^{\circ}\text{C}$, black dots in Fig. 11) weakens the correlation between the global temperatureGMST and the North American ice volume/southern extent to -0.193 and -0.285 , respectively. Nevertheless, the correlation analysis still shows some sensitivity of the southern extent of the North American ice sheet to global temperatureGMST (Fig. 11b), where a colder global climate tends to produce a more extensive ice sheet in the south. In other words, it can also be said that it is hard to get an extensive southern North American ice sheet under warm LGM global temperatureGMST (above 12.0°C), irrespective of the albedo parameters, which demonstrates the value of constraining the upper band of real LGM temperatures for simulating the North American ice sheet well.

The Greenland ice sheet appears to be insensitive to the reasonable LGM global temperatureGMST range (2.7°C - 14.7°C), which is consistent with the dominant role of basal sliding in controlling the ice volume. Reducing the uncertainty level to two sigma ($8.7^{\circ}\text{C} \pm 4.0^{\circ}\text{C}$, black dots in Fig. 11) increases the correlation value to 0.259 possibly associated with an

545 increase in snow fall following the warming climate, however the effect is much weaker compared to the effect of basal
546 sliding.



547

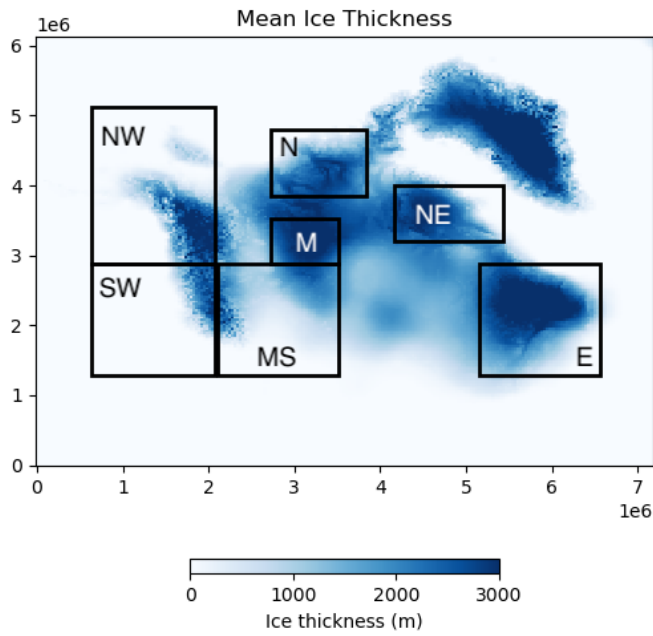
548

549 Fig. 11 Relationship between [global mean annual surface air temperature GMST](#) [°C] and Ice sheet variables. (a) North
550 American ice sheet volume [m], (b) Ratio of southern extent of the North American ice sheet compared to Dalton et al.
551 (2020) and (c) Greenland ice sheet volume [m]. Ensemble members that satisfy the [global temperature GMST](#) constraint and
552 have run 5000 ice sheet years are used (87 members). Correlation values are also shown in each figure. Black dots show
553 results within the two sigma uncertainty in the LGM [global temperature GMST](#) ($8.7^{\circ}\text{C} \pm 4.0^{\circ}\text{C}$).
554

555

555 [3.5 Localities in the effect of parameters](#)

556 [The different sensitivities to parameters between the North American and Greenland ice sheets imply that similar variations](#)
557 [in sensitivity to parameters may exist between different local regions within the huge North American ice sheet. To explore](#)
558 [this point, we separate the North American ice sheet into seven different sectors \(NW, SW, N, M, MS, NE, E\) where a](#)
559 [substantial amount of ice remains in the ensemble mean of members satisfying the GMST constraint \(Fig. 12\). Results are](#)
560 [summarized in Table 2. While the albedo parameters remain the most important ones \(*daice* and *avgr*\) in each region, we](#)
561 [find that *beta* has an increased influence in SW and M. These areas either exhibit a mountainous bedrock topography or have](#)
562 [very thick ice, hence can be more affected by the basal sliding parameters. Additionally, we find that *ct* has a relatively](#)
563 [strong influence on the northern \(N\) and eastern \(E\) parts of the North American ice sheet. Our analysis indicates some](#)
564 [variation in regional sensitivities to climate and ice sheet parameters in different sectors of the ice sheet sectors. Further](#)
565 [analysis beyond the scope of this study would be required to explore this regional dependency in detail.](#)



566

567 [Fig. 12 Six different areas \(NW, SW, N, M, NE and E\) of the North American ice sheet used for the additional analysis](#)
 568 [\(black rectangle\). Blue shades show the mean ice thickness \[m, colour\] of members satisfying the GMST constraint.](#)

569

570 [Table 2 Four most influential parameters on ice volumes at different regions. Values in the bracket show the correlation. For](#)
 571 [the Southern Extent, results from Fig. S4 are used.](#)

<u>Region</u>	<u>1</u>	<u>2</u>	<u>3</u>	<u>4</u>
<u>NW</u>	avgr (-0.48)	fsnow (0.47)	daice (0.4)	ct (-0.25)
<u>SW</u>	fsnow (0.42)	daice (0.4)	beta (0.39)	avgr (-0.35)
<u>N</u>	avgr (-0.44)	daice (0.37)	ct (-0.36)	fsnow (0.28)
<u>M</u>	daice (0.53)	avgr (-0.49)	beta (0.29)	ct (-0.25)
<u>MS</u>	avgr (-0.58)	daice (0.47)	fsnow (0.39)	ct (-0.30)
<u>NE</u>	avgr (-0.52)	daice (0.49)	smb (0.30)	fsnow (0.26)
<u>E</u>	avgr (-0.48)	daice (0.43)	fsnow (0.33)	ct (-0.30)
<u>Southern Extent</u>	avgr (-0.52)	daice (0.41)	fsnow (0.36)	ct (-0.33)

572

573 **[3.6 Sensitivity of influential parameters to individual constraints](#)**

574 [Applying our three simulation constraints simultaneously may be hiding relationships that exist between model parameters](#)
 575 [and simulation behaviour. We perform additional analyses to explore how each constraint individually affects the](#)
 576 [relationship between our model parameters and North American ice sheet volume. In the case of no-constraints \(139](#)
 577 [members\), the albedo parameters are important, but the influence from *ct* becomes more important \(Table 3\). This is due to](#)
 578 [the increased range of GMST allowed by varying *ct* \(Fig. 5\). Having a much colder or warmer climate allows the ice sheets](#)
 579 [to grow or melt, and the resulting feedback further enhances the role of *ct*. In contrast, most members with extremely warm](#)
 580 [climates crashed during the 5000 year simulation. This means that, *entcoef* does not appear to have so large an effect on ice](#)
 581 [sheet volume directly, unlike its importance in setting the GMST.](#)

582

583 In the case of applying only the ice sheet volume constraint (73 members), *avgr* and *fsnow* still show relatively high
 584 correlations with ice sheet volume. However their influence is less than when GMST constraint alone is applied (Table 3).
 585 The ice volume constraint alone results in a preferred selection of members exhibiting colder climates (46 members have a
 586 GMST below 4 °C). As a result, the members are less sensitive to albedo related parameters.

587
 588 When the southern extent constraint alone is applied, 33 members remain. Similar to above, members satisfying this
 589 condition tend to have very cold climates, where 24 members have GMST colder than 4°C and 14 members colder than
 590 0.63°C. In this case, *avgr* and *beta* appear to be most influential. This may imply that snow albedo and basal conditions play
 591 an important role in maintaining an extensive ice sheet once the climate allows the ice sheet to reach this size. Further
 592 discussion on the maintenance of the southern margin of the North American ice sheet is in subsection 4.1.

593
 594 Table 3 Effects of constraints on the relation of parameters and North American ice sheet volume at year 5000. The four
 595 most influential parameters on ice volumes are shown.

<u>Constraint applied</u>	<u>1</u>	<u>2</u>	<u>3</u>	<u>4</u>
<u>No Constraint</u> <u>(139 members)</u>	<u><i>daice</i> (0.51)</u>	<u><i>avgr</i> (-0.45)</u>	<u><i>ct</i> (0.45)</u>	<u><i>fsnow</i> (0.35)</u>
<u>GMST alone</u> <u>(87 members)</u>	<u><i>avgr</i> (-0.56)</u>	<u><i>daice</i> (0.48)</u>	<u><i>fsnow</i> (0.37)</u>	<u><i>ct</i> (-0.33)</u>
<u>Min Ice volume</u> <u>alone</u> <u>(73 members)</u>	<u><i>avgr</i> (-0.39)</u>	<u><i>fsnow</i> (0.33)</u>	<u><i>smb</i> (0.33)</u>	<u><i>daice</i> (0.24)</u>
<u>Southern Extent alone</u> <u>(33 members)</u>	<u><i>avgr</i> (-0.71)</u>	<u><i>beta</i> (0.51)</u>	<u><i>smb</i> (0.44)</u>	<u><i>fsnow</i> (0.39)</u>

596
 597
 598

599 **4. Discussion**

600 **4.1 How could FAMOUS-BISICLES be made to reproduce the southern extent of the North American ice sheet?**

601 A recent study by Gandy et al. (2023) performed a similar ensemble simulation with FAMOUS-GLIMMERIce, but with
 602 fixed SSTs ~~instead of FAMOUS~~ and with the simpler Glimmer ice sheet model rather than BISICLES ~~coupled to a slab~~
 603 ~~ocean model used in this study.~~ Our findings here are consistent with ~~them~~theirs in that the ice extent is sensitive to choices
 604 of parameters in the snow and ice albedo scheme and that both models underestimate the southern extent of the North
 605 American ice sheet, especially the so-called ‘lobe’ characteristics. To investigate the possibility of the model being able to
 606 reproduce the full extent of the southern margin of the North American ice sheet, we analyse in detail the ensemble member
 607 that has the most extensive southern margin, disregarding our imposed climate plausibility constraints (Fig. 3e). In ~~the~~this
 608 simulation, the performance of the southern extent of the North American ice sheet ~~improves and becomes~~is closer to the
 609 reconstructed area due to the very cold climate ~~simulated~~, whose absolute ~~global temperature~~GMST is -7.4°C. Yet even in
 610 this very cold simulation, the model cannot maintain the ‘lobe’ characteristics of the North American ice extent as far south
 611 as the reconstructions.

612

613 So, how might we reproduce the southern margin of the North American ice sheet? in our simulations? There are several
614 possibilities:

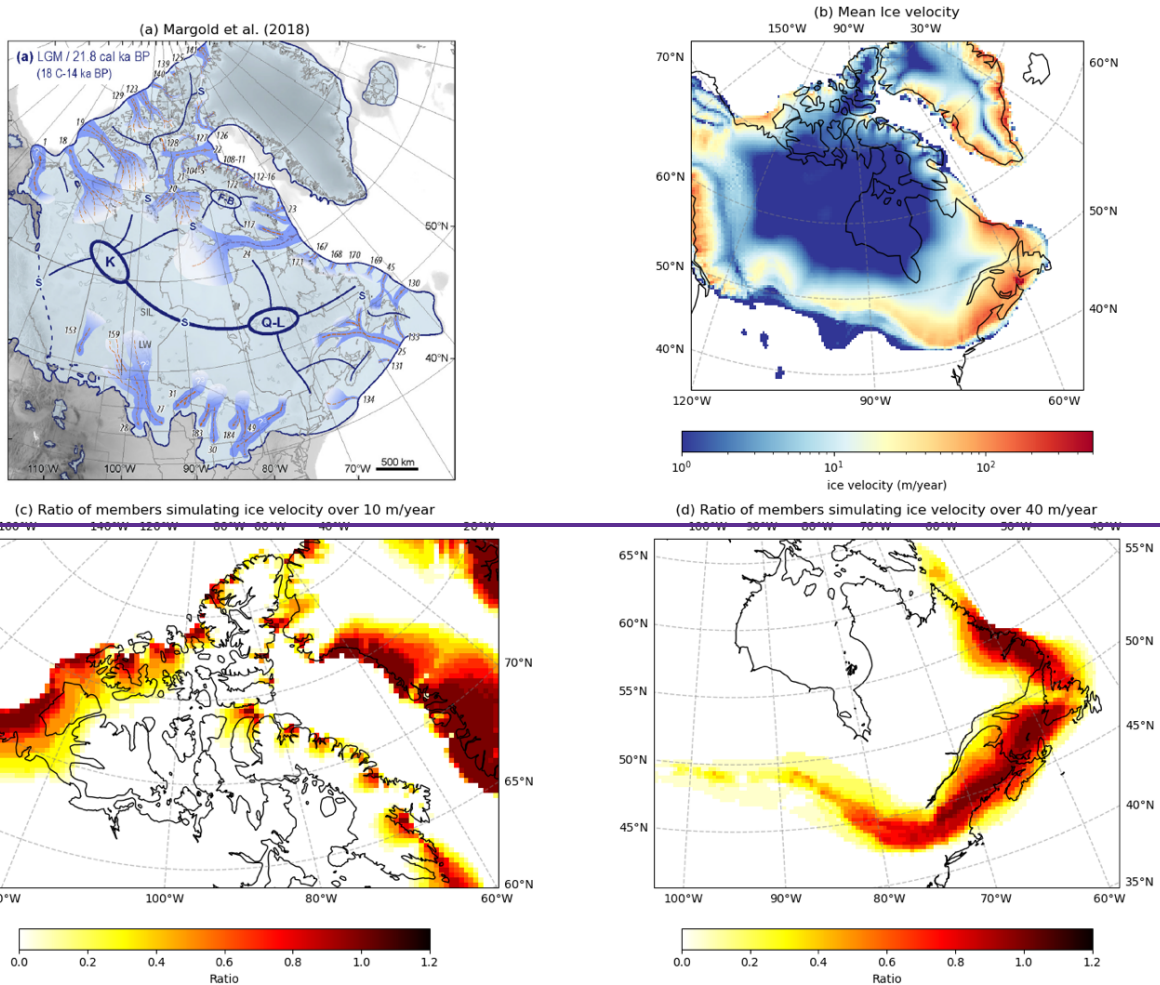
- 615 • Finer horizontal resolution in the climate model: during the simulations, FAMOUS-BISICLES loses the thin ice
616 sheet at the south margin abruptly in the first 1000 ice sheet years due to the very large negative SMB simulated in
617 the atmospheric model (e.g. Fig. 13b). ~~As discussed above, applying~~ Applying a high-resolution atmospheric model
618 might be better able to sustain a more southerly ice margin through a stronger stationary wave effect that cools the
619 area (Abe-Ouchi et al. 2007).
- 620 • Representation of clouds: Gregory et al. (2012) pointed out the importance of changes in cloud cover over the
621 southern margin of the North American ice sheet on its SMB during the glacial inception. Having a larger cloud
622 cover at the southern margin may help to maintain the ice sheet by reducing the very large negative SMB,
623 ~~while~~ although a careful analysis on the physical plausibility ~~needs of creating this feature would need~~ to be done.
- 624 • Improvements in the downscaling scheme: including the effect of strongly stratified boundary layer on the surface
625 temperature during the downscaling may allow a colder surface temperature over ice, which can help sustain the ice
626 sheet at its margin. Incorporation of downscaling of accumulation in FAMOUS-BISICLES can increase the snow
627 fall at the southern margin, which increases the SMB and surface albedo and may help to sustain the ice sheet at the
628 southern margin (e.g. Yamagishi and Abe-Ouchi 2005).
- 629 • Higher initial surface elevation: the simulation could be started with a higher initial surface elevation which can be
630 obtained by giving a thicker ice or a higher bedrock topography at the southern margin, allowing for lower surface
631 temperatures due to the higher elevation, although this may not be physically plausible.
- 632 • Palaeo-vegetation: the choice of vegetation type for the unglaciated region near to the ice sheet may be relevant.
633 The modern vegetation distribution used in this study may tend to give a warmer condition in this area, unlike
634 tundra, which grows under cold climates and causes a surface cooling (O'ishi and Abe-Ouchi 2013).
- 635 • Bedrock conditions: creating a slippery bedrock condition would enhance ice flow from the ice sheet interior
636 towards the margin, and so may be instrumental in redistributing ice outwards. In this regard, adding a scheme that
637 allows the generation of proglacial lakes and increases ice flow at the southern margin would help advance the lobe
638 (Hinck et al. 2022).
- 639 • Longer integration of the model: extending the integration of FAMOUS-BISICLES may help to redistribute the
640 thick ice in the interior to the southern margin. In fact, some of the members, which have been extended for
641 additional 5000 years show ~~asome~~ southward expansion (Fig. S2).

642 It is also possible that the concept of the southern margin being in a quasi-equilibrium state with the LGM forcing may not
643 be valid, and that ~~it~~ may instead be ~~reflecting~~ several transient ice ~~advancing~~ advance events that occurred during the recent
644 glacial period (and preceding the LGM)(e.g. Pico et al. 2017, Gowan et al. 2021, Bradley et al. ~~2023~~2024). We speculate that
645 such earlier southward ice advance may allow a more expansive southern ice sheet to establish, before rebalancing with the
646 insolation forcing. In this case, running a long transient simulation, rather than performing equilibrium-type LGM
647 simulations, may be essential for achieving the target southern margin extent.

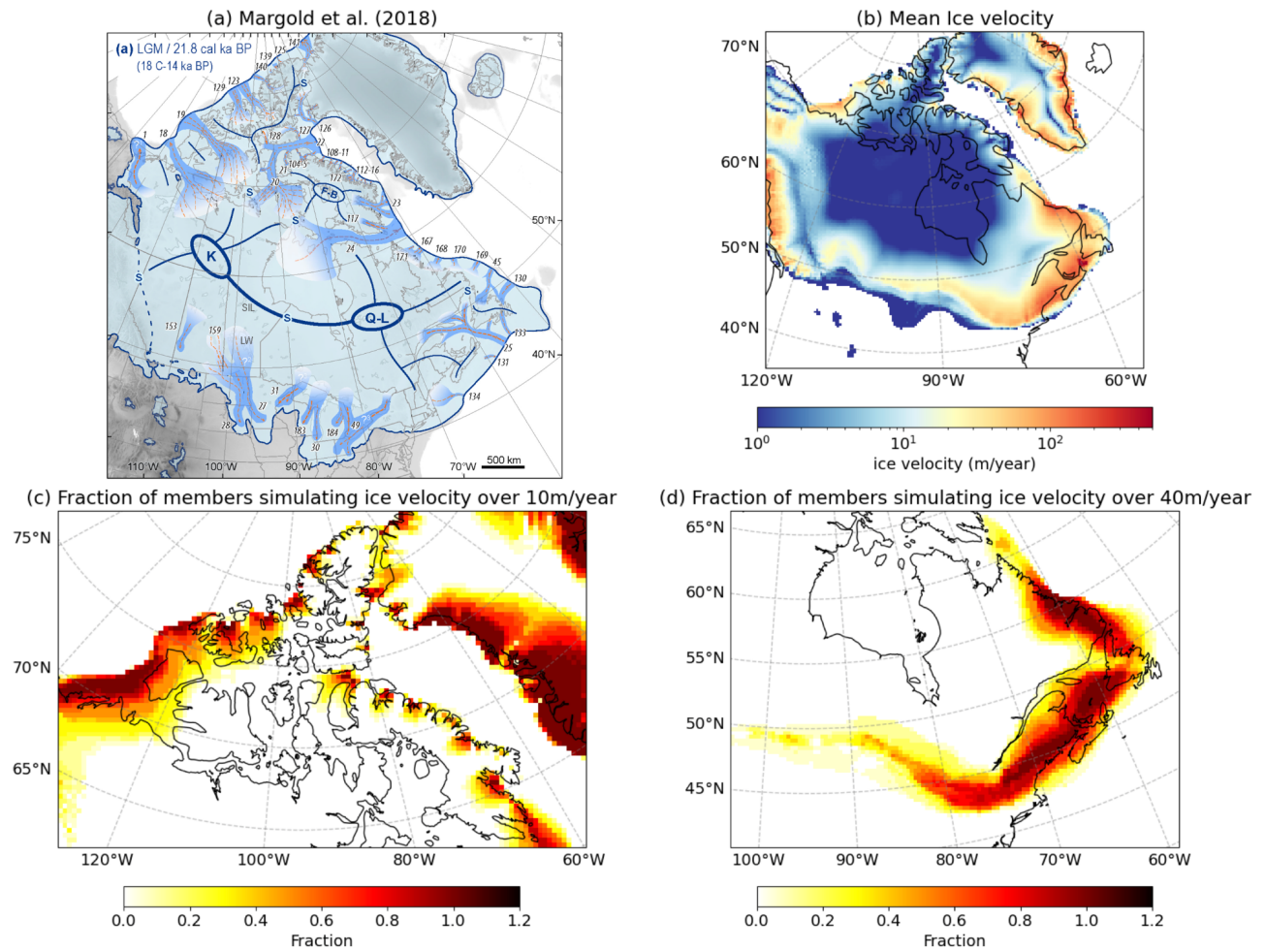
648 4.2 Performances of ice streams

649 The positions of our simulated ice streams in the best sixteen ensemble members are evaluated against the reconstruction by
650 Margold et al. (2018) (Fig. ~~4213~~ and Fig. S5). The figure depicts that BISICLES shows regions of relatively high ice
651 velocities (or ice streams) at various sites, despite the relatively low resolution of the model (16 km at finest grid) and the
652 relatively short integration period. Specifically, most members reproduce high ice velocities at the margin over the Baffin
653 Bay area. In addition, the simulation of ice streams facing the Arctic Ocean is encouraging (Fig. ~~4213~~, S5). However, once
654 again the southern margin is tricky to get right, and our ice stream behaviour there is somewhat diffuse, not picking up the

655 characteristic ‘lobe’ structure of the reconstructions (Margold et al. 2018). Over the Eastern North American ice sheet, the
 656 model captures some large glaciers such as Laurentian Channel (25), Placentia Bay-Halibut Channel (133) and Hopedale
 657 Saddle (168), while none of the best sixteen ensemble members simulate the large ice stream that flows to the Labrador Sea
 658 from the present-day Hudson Bay area. These poorly represented ice stream features may be caused by low resolution of the
 659 smallest ice sheet refinement (16 km, e.g. Gandy et al. 2019), too-short integration and misrepresentation of the surface type
 660 of till (Gowan et al. 2019). With the last point, the amount of till water calculated prognostically in the simulations appears
 661 small, hence most areas use the Weertman sliding law. An increase in the basal melting, a choice of a smaller value for
 662 *drain* or incorporating a spatially variable Weertman coefficient map based on geological evidence may help to improve the
 663 performance of the ice streams. Nevertheless, the model does show some reasonable potential in simulating North American
 664 ice streams considering the relatively low resolution as well as the explicit calculation of basal drag.
 665



666
 667



668

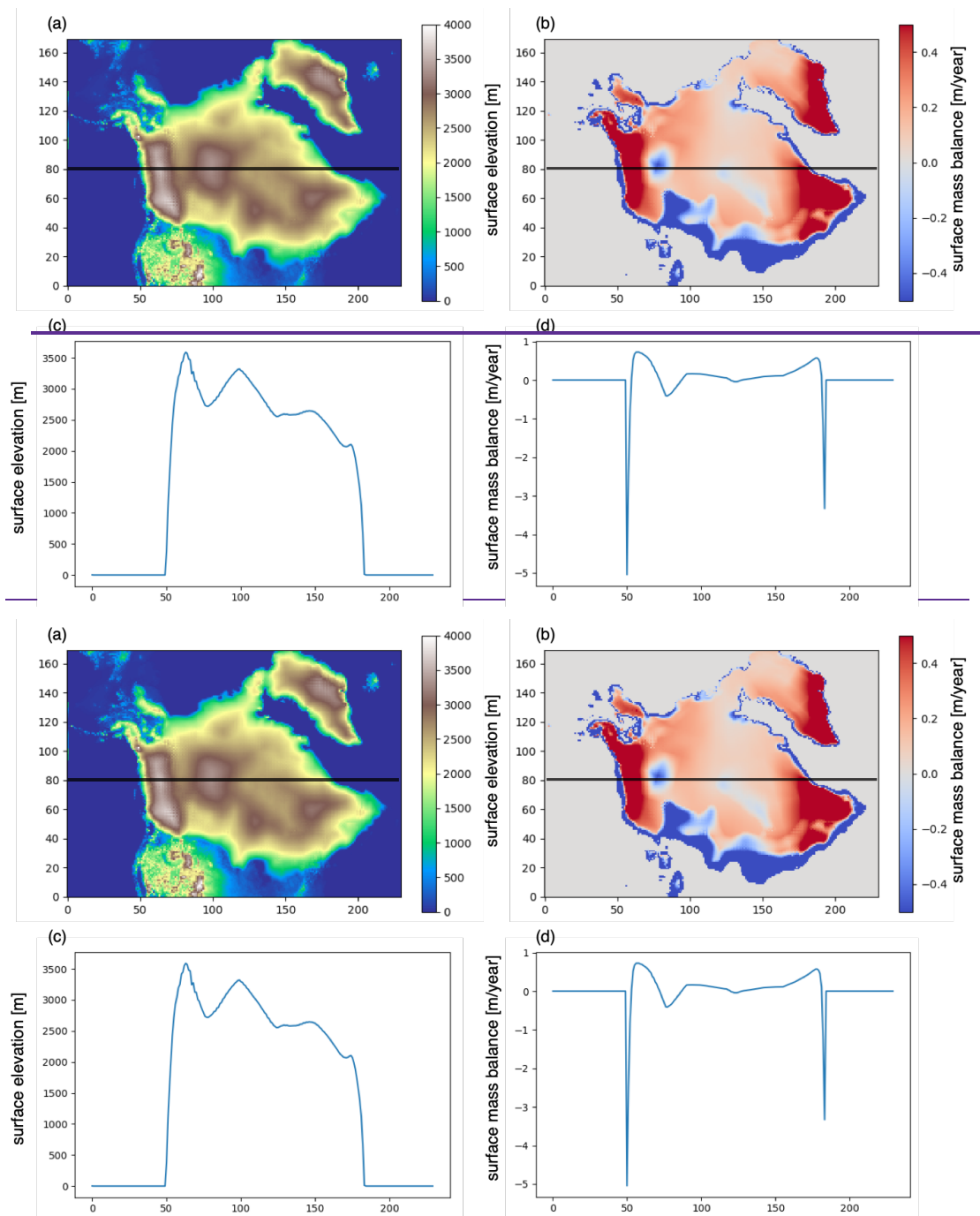
669 Fig. 12-13 Comparison of ice velocity [m/year, colour] between (a) Reconstruction (Margold et al. 2018, adapted from Fig. 5
 670 of Margold et al. 2018) and (b) the mean of best sixteen members. (c) and (d) show the ratio fraction of numbers of members
 671 simulating ice velocity beyond 10m/year for (c) and 40m/year for (d), respectively. Ratio Fraction of 1.0 means all the
 672 sixteen members simulate ice velocities of those values.

673 **4.3 Effects of biases in the simulated climate**

674 Some of the simulations in the ensemble exhibit a local melting of the ice sheet from parts of the interior outwards, which is
 675 unusual, as ice sheets usually melt from their margins, where the surface temperature is close to the freezing point (e.g. Figs
 676 3c and 13-14). This phenomenon is caused by biases in the atmospheric model, which are then amplified by the downscaling
 677 method and a positive feedback from the coupling. First in these simulations, the model has a warm summer temperature bias
 678 over the ice sheet interior. As a result, large parts of the central North American ice sheet have a temperature above -10°C
 679 despite the surface elevation exceeding 2000 m (Fig. 10). A similar feature was pointed out by Smith et al. (2021) using the
 680 same model under the modern Greenland ice sheet, which produced a higher ELA (around 2 km high in places) compared to
 681 a high resolution regional atmospheric model (at about 1 km high). Second, because the downscaling of SMB strongly
 682 depends on the elevation, a local change in surface elevation can induce a local negative surface mass balance if the surface
 683 temperature calculated in the FAMOUS grid points are close to the freezing point. This example is shown in Fig. 13-14,
 684 where a negative SMB can be found at the local minimums/minima of surface elevation, despite the elevation exceeding
 685 2000 m. The initial negative SMB then kicks in a strong positive feedback where melting of snow reduces the albedo and
 686 results in more energy absorption. As a result, the ice elevation starts to decrease and causes additional positive feedback
 687 similar to saddle node collapse (Gregoire et al. 2012). This The strong dependence of SMB on temperature and altitude

688 [implied by this](#) way of downscaling the climate model output works well for modern Greenland, especially at low elevation
 689 where the SMB [has been observed to have a](#) very strong elevation dependence. However, at the higher altitudes achieved by the
 690 LGM North American ice sheet, SMB may be more greatly affected by other factors such as wind speeds, as suggested by
 691 studies on Antarctica (Van Liefferinge et al. 2021). Hence, further improvements in the downscaling method at higher
 692 elevation could help to reduce the impact of the climate biases.

693



694

695

696 Fig. 13-14 An example of local ice melting in the interior of the ice sheet; [ensemble member xplji](#), which has a GMST of
 697 [9.9°C](#) and North American ice sheet volume of 88.4m SLE. (a) Surface topography [m] and (b) Surface mass balance
 698 [m/year]. Height zonal cross-section of (c) surface topography and (d) surface mass balance at y=80 are shown.

699 **5. Conclusion**

700 In this paper, we have presented a large ensemble of simulations of the North American and Greenland ice sheets and
 701 climate of the LGM, performed with a coupled atmosphere-ice sheet-slab ocean model FAMOUS-BISICLES, a version of

702 the FAMOUS-~~ice~~Ice model developed by Smith et al. (2021). The experiment consists of a 200-member perturbed parameter
703 ensemble, where the values of 16 parameters associated with climate and ice dynamics were varied using a Latin-hypercube
704 sampling method. The simulated results are evaluated against the LGM ~~global mean surface air temperature~~GMST, the
705 North American ice volume and the southern extent of the North American ice sheet. In the ensemble, the ~~global~~
706 ~~temperature~~GMST is controlled by a combination of precipitation efficiency in the large-scale condensation and entrainment
707 rate in the cumulus convection, consistent with previous FAMOUS simulations of modern climate (Joshi et al. 2010). Under
708 reasonable LGM ~~global temperature~~GMST conditions, we find that the surface albedo exerts the strongest control on North
709 American ice volume. In contrast, the ice volume of Greenland is found to be mainly controlled by the Weertman coefficient
710 in the basal sliding law. The different sensitivity of these ice sheets to the model's physical parameter values mainly comes
711 from different climatic conditions; the North American ice sheet being generally warmer hence has a larger area of negative
712 SMB, which is affected by the albedo. In contrast, most parts of the Greenland ice sheet are covered by a very cold
713 atmosphere, hence the ice sheet volume is more affected by the calving at its margin, the total amount of which is controlled
714 by the magnitude of the basal sliding law that affects the amount of ice transported to the margins. These differences
715 between the North American and Greenland ice sheets provide an important take-home message on model performance,
716 suggesting that for best flexibility (i.e., the ability to simulate conditions ~~largely~~very different from today), simulators should
717 be calibrated under ~~substantially different~~a range of climate and ice sheet conditions and tested out-of-sample.

718
719 Analysis of the relationship between the North American southern ice extent and ~~global temperature~~GMST with the
720 uncertainty level of two sigmas ($8.7^{\circ}\text{C} \pm 4.0^{\circ}\text{C}$) shows a slightly weak relation. Nevertheless, we find that it is hard to get an
721 extensive southern North American ice sheet under warm LGM global temperature (above 12.0°C), irrespective of the
722 albedo parameters in our model. This demonstrates the value of constraining the upper band of real LGM temperatures for
723 simulating the North American ice sheet well.

724
725 Based on our plausibility constraints, the model produces sixteen 'acceptable' simulations with reasonable ~~global~~
726 ~~temperature~~GMST and North American ice sheet. These simulations show the most extensive southern margin under
727 reasonable LGM temperature and ice volume, but, ~~as with many like~~ LGM ice sheet simulations, ~~are not sufficiently~~
728 ~~expansive at the southern margin and- by other authors, they~~ overestimate ice volume in Alaska, ~~and do not expand far~~
729 ~~enough at the southern margin (even after 5000 years, with the absolute global temperature as cold as -7.4°C).~~ . Both of
730 these features are likely attributable to the underestimation of the stationary wave effect (Roe and Lindzen 2001, Abe-Ouchi
731 et al. 2007), ~~and may which might~~ be improved upon/overcome by increasing the climate model resolution. ~~We find that the~~
732 ~~model cannot reproduce the southern margin of the ice sheet over the 5000-year simulation even if the absolute global~~
733 ~~temperature is as cold as -7.4°C , and it~~ It is also possible that more accurate representation of the palaeo vegetation, different
734 treatments of ice sheet sliding and downscaling method of the SMB, or a different spin-up procedure could improve the
735 simulated ~~southerly~~southward ice sheet ~~extent~~extension.

736
737 Our results show that warm summer temperature biases in the interior of the ice sheet as well as the downscaling method of
738 SMB based on elevation can cause strong local melting of the ice sheet from the interior outwards. More complex treatment
739 of the atmospheric conditions and surface mass balance in the ice sheet interior could improve this, and may be especially
740 important when applying the model to the Antarctic ice sheet.

741
742 Lastly, the strong sensitivities of the North American ice sheet to albedo at the LGM may imply a potential constraint on the
743 future Greenland ice sheet by constraining the formulation and behaviour of albedo schemes for climate and ice sheet models
744 under relatively warm climates. Running similar ensemble simulations ~~with a directly comparable version of this model~~ for

745 the modern and future Greenland ice sheet will provide an important data set to directly connect the simulations of past
746 climates and ice sheets to those of the modern and future. Using such data, we maywill be able to explore whetherhow
747 simulations of past climate-ice sheet conditions can more tightly constrain or increase the confidence of projectionin
748 projections of future sea level rise.

749 **Code and data availability**

750 The simulation data of FAMOUS-BISICLES used in this study will be -available in a public database.

751 **Author contribution**

752 Sam Sherriff-Tadano (Data curation, Formal Analysis, Investigation, Methodology, Validation, Visualization, Writing-
753 original draft), Ruza Ivanovic (Conceptualisation, Funding Acquisition, Investigation, Methodology, Project Administration,
754 Resources, Software, Supervision, Writing - review and editing), Lauren Gregoire (Conceptualisation, Funding Acquisition,
755 Investigation, Methodology, Project Administration, Resources, Software, Supervision, Writing - review and editing),
756 Charlotte Lang (Data curation, Formal Analysis, Investigation, Methodology, Writing-review and editing), Niall Gandy
757 (Data curation, Formal Analysis, Investigation, Methodology, Writing-review and editing), Tamsin Edwards (Funding
758 acquisition, Methodology, Writing – original draft). Robin S. Smith (Conceptualisation, Funding Acquisition, Methodology,
759 Project Administration, Resources, Software, Supervision, Writing - review and editing), Jonathan Gregory
760 (conceptualization, funding acquisition, methodology, software, writing - review and editing), Oliver Pollard (Methodology,
761 Visualization, Writing - review and editing)

762 **Competing interest**

763 The authors declare no competing interests.

764 **Acknowledgements**

765 This work was undertaken on ARC4, part of the High Performance Computing Facilities at the University of Leeds,
766 ARCHER2 and JASMIN. RFI, RSS, JG, TE, CL and SST were funded by “RiSICMAP”, NERC Standard Grant
767 NE/T007443/1. NG, LJG, RFI were funded by “SMB-Gen” UKRI Future Leaders Fellowship MR/S016961/1. SST was
768 funded by JSPS. We are also grateful to Richard Rigby for his assistance in setting up the simulation. SST also thanks Ayako
769 Abe-Ouchi, Miren Vizcaino, Heiko Goelzer and Jonathan Owen for constructive discussion.

770 **References**

- 771 Abe-Ouchi, A., et al.: Ice-sheet configuration in the CMIP5/PMIP3 Last Glacial Maximum experiments. *Geoscientific*
772 *Model Development*, 8, 3621-3637. <https://doi.org/10.5194/gmd-8-3621-2015>, 2015.
- 773 Abe-Ouchi, A., et al.: Insolation-driven 100,000-year glacial cycles and hysteresis of ice-sheet volume. *Nature*, 500, 190-+.
774 <https://doi.org/10.1038/nature12374>, 2013.
- 775 Abe-Ouchi, A., Segawa, T., & Saito, F.: Climatic Conditions for modelling the Northern Hemisphere ice sheets throughout
776 the ice age cycle. *Climate of the Past*, 3, 423-438. <https://doi.org/10.5194/cp-3-423-2007>, 2007.
- 777 Alder, J.R., Hostetler, S.W.: Applying the Community Ice Sheet Model to evaluate PMIP3 LGM climatologies over the
778 North American ice sheets. *Clim Dyn* 53, 2807–2824. <https://doi.org/10.1007/s00382-019-04663-x>
779 <https://doi.org/10.1007/s00382-019-04663-x>, 2019.
- 780 Blasco, J., Alvarez-Solas, J., Robinson, A., and Montoya, M.: Exploring the impact of atmospheric forcing and basal drag on
781 the Antarctic Ice Sheet under Last Glacial Maximum conditions, *The Cryosphere*, 15, 215–231.
782 <https://doi.org/10.5194/te-15-215-2021> <https://doi.org/10.5194/tc-15-215-2021>, 2021.
- 783 Braconnot, P. et al.: Evaluation of climate models using palaeoclimatic data. *Nature Climate Change* 2, 417-424.

<https://doi.org/10.1038/nclimate1456>~~https://doi.org/10.1038/nclimate1456~~, 2012.

Braconnot, P. et al.: Results of PMIP2 coupled simulations of the Mid-Holocene and Last Glacial Maximum - Part 1: experiments and large-scale features. *Climate of the Past* 3, 261-277. 2007.

Bradley, S. L., Reerink, T. J., van de Wal, R. S. W., and Helsen, M. M.: Simulation of the Greenland Ice Sheet over two glacial–interglacial cycles: investigating a sub-ice- shelf melt parameterization and relative sea level forcing in an ice-sheet–ice-shelf model, *Clim. Past*, 14, 619–635. ~~https://doi.org/10.5194/cp-14-619-2018~~<https://doi.org/10.5194/cp-14-619-2018>, 2018.

Bradley, S. L., Sellevold, R., Petrini, M., Vizcaino, M., Georgiou, S., Zhu, J., Otto-Bliesner, B. L., and Lofverstrom, M.: Surface mass balance and climate of the Last Glacial Maximum ~~northern hemisphere~~[Northern Hemisphere](https://doi.org/10.5194/cp-2023-62) ice sheets: simulations with CESM2.1, *Clim. Past Discuss. [preprint]*, 20, 211–235, ~~https://doi.org/10.5194/cp-2023-62, in review, 2023~~<https://doi.org/10.5194/cp-2023-62>, 2024.

Briggs, R. D., Pollard, D., and Tarasov, L.: A data-constrained large ensemble analysis of Antarctic evolution since the Eemian, *Quatern. Sci. Rev.*, 103, 91–115. ~~https://doi.org/10.1016/j.quascirev.2014.09.003~~<https://doi.org/10.1016/j.quascirev.2014.09.003>, 2014.

Clark, P. U. et al.: The Last Glacial Maximum. *Science* 325, 710-714.

~~https://doi.org/10.1126/science.1172873~~<https://doi.org/10.1126/science.1172873>, 2009.

Clark, P. U. and Mix, A. C.: Ice sheets and sea level of the Last Glacial Maximum, *Quaternary Science Reviews*, Volume 21, Issues 1–3, 2002, Pages 1-7. [https://doi.org/10.1016/S0277-3791\(01\)00118-4](https://doi.org/10.1016/S0277-3791(01)00118-4), 2002.

Cornford, S. L., Martin, D. F., Graves, D. T., Ranken, D. F., Le Brocq, A. M., Gladstone, R. M., Payne, A. J., Ng, E. G., Lipscomb, W. H.: Adaptive mesh, finite volume modeling of marine ice sheets, *Journal of Computational Physics*, Volume 232, Issue 1, 2013, Pages 529-549. <https://doi.org/10.1016/j.jcp.2012.08.037>, 2013.

Dalton, A. S. et al.: An updated radiocarbon-based ice margin chronology for the last deglaciation of the North American Ice Sheet Complex, *Quaternary Science Reviews*, Volume 234, 106223, ISSN 0277-3791, <https://doi.org/10.1016/j.quascirev.2020.106223>, 2020.

DeConto, R., Pollard, D.: Contribution of Antarctica to past and future sea-level rise. *Nature* 531, 591–597. <https://doi.org/10.1038/nature17145>, 2016.

Dyke, A.S. et al.:The Laurentide and Innuitian ice sheets during the Last Glacial Maximum, *Quaternary Science Reviews*, Volume 21, Issues 1–3, Pages 9-31, ISSN 0277-3791, [https://doi.org/10.1016/S0277-3791\(01\)00095-6](https://doi.org/10.1016/S0277-3791(01)00095-6), 2002.

Edwards, T. L. et al.: Projected land ice contributions to twenty-first-century sea level rise. *Nature* 593, 74+.
<https://doi.org/10.1038/s41586-021-03302-y>, 2021.

Gandy, N. et al.: Marine ice sheet instability and ice shelf buttressing of the Minch Ice Stream, northwest Scotland. *Cryosphere* 12, 3635-3651. <https://doi.org/10.5194/tc-12-3635-2018>, 2018.

Gandy, N. et al.: Exploring tile ingredients required to successfully model the placement, generation, and evolution of ice streams in the British-Irish Ice Sheet. *Quaternary Science Reviews* 223. <https://doi.org/10.1016/j.quascirev.2019.105915>, 2019.

Gandy, N., Gregoire, L. J., Ely, J. C., Cornford, S. L., Clark, C. D., & Hodgson, D. M.: Collapse of the last Eurasian Ice Sheet in the North Sea modulated by combined processes of ice flow, surface melt, and marine ice sheet instabilities. *Journal of Geophysical Research: Earth Surface*, 126, e2020JF005755. <https://doi.org/10.1029/2020JF005755>, 2021.

Gandy, N., Astfalck, L. C., Gregoire, L. J., Ivanovic, R. F., Patterson, V. L., Sherriff-Tadano, S., et al.: De-tuning albedo parameters in a coupled Climate Ice Sheet model to simulate the North American Ice Sheet at the Last Glacial Maximum. *Journal of Geophysical Research: Earth Surface*, 128, e2023JF007250. <https://doi.org/10.1029/2023JF007250>, 2023.

- 827 Golledge, N. R. et al.: Global environmental consequences of twenty-first-century ice-sheet melt. *Nature* 566, 65–+.
828 <https://doi.org/10.1038/s41586-019-0889-9>, 2019.
- 829 Gowan, E. J. et al.: A new global ice sheet reconstruction for the past 80000 years. *Nature Communications* 12.
830 <https://doi.org/10.1038/s41467-021-21469-w>, 2021.
- 831 [Gowan, E. J., Niu, L., Knorr, G., and Lohmann, G.: Geology datasets in North America, Greenland and surrounding areas
832 for use with ice sheet models, *Earth Syst. Sci. Data*, 11, 375–391, <https://doi.org/10.5194/essd-11-375-2019>, 2019.](https://doi.org/10.5194/essd-11-375-2019)
- 833 Gregoire, L. J., Ivanovic, R. F., Maycock, A. C., Valdes, P. J. & Stevenson, S.: Holocene lowering of the Laurentide ice
834 sheet affects North Atlantic gyre circulation and climate. *Climate Dynamics* 51, 3797-3813.
835 <https://doi.org/10.1007/s00382-018-4111-9>, 2018.
- 836 Gregoire, L. J., Payne, A. J. & Valdes, P. J.: Deglacial rapid sea level rises caused by ice-sheet saddle collapses. *Nature* 487,
837 219-U1506. <https://doi.org/10.1038/nature11257>, 2012.
- 838 Gregoire, L. J., Valdes, P. J., Payne, A. J. & Kahana, R.: Optimal tuning of a GCM using modern and glacial constraints.
839 *Climate Dynamics* 37, 705-719. <https://doi.org/10.1007/s00382-010-0934-8>, 2011.
- 840 Gregory, J. M., Browne, O. J. H., Payne, A. J., Ridley, J. K. & Rutt, I. C.: Modelling large-scale ice-sheet-climate
841 interactions following glacial inception. *Climate of the Past* 8, 1565-1580. <https://doi.org/10.5194/cp-8-1565-2012>,
842 2012.
- 843 Gregory, J. M., George, S. E. & Smith, R. S.: Large and irreversible future decline of the Greenland ice sheet. *Cryosphere*
844 14, 4299-4322. <https://doi.org/10.5194/tc-14-4299-2020>, 2020.
- 845 [Hinck, S., Gowan, E. J., Zhang, X., and Lohmann, G.: PISM-LakeCC: Implementing an adaptive proglacial lake boundary in
846 an ice sheet model, *The Cryosphere*, 16, 941–965, <https://doi.org/10.5194/tc-16-941-2022>, 2022.](https://doi.org/10.5194/tc-16-941-2022)
- 847 Holden, P.B., Edwards, N.R., Oliver, K.I.C. *et al.*: A probabilistic calibration of climate sensitivity and terrestrial carbon
848 change in GENIE-1. *Clim Dyn* 35, 785–806. <https://doi.org/10.1007/s00382-009-0630-8>, 2010.
- 849 Hughes, A. L. C., Gyllencreutz, R., Lohne, Ø. S., Mangerud, J., Svendsen, J. I.: The last Eurasian ice sheets – a
850 chronological database and time-slice reconstruction, DATED-1. *Boreas*, Vol 45, pp. 1– 45. [10.1111/bor.12142](https://doi.org/10.1111/bor.12142). ISSN
851 0300-9483, 2016.
- 852 [IPCC, 2021: *Climate Change 2021: The Physical Science Basis. Contribution of Working Group I to the Sixth Assessment
853 Report of the Intergovernmental Panel on Climate Change*\[Masson-Delmotte, V., P. Zhai, A. Pirani, S.L. Connors, C.
854 Péan, S. Berger, N. Caud, Y. Chen, L. Goldfarb, M.I. Gomis, M. Huang, K. Leitzell, E. Lonnoy, J.B.R. Matthews, T.K.
855 Maycock, T. Waterfield, O. Yelekçi, R. Yu, and B. Zhou \(eds.\)\]. Cambridge University Press, Cambridge, United
856 Kingdom and New York, NY, USA, In press, doi:10.1017/9781009157896, 2021.](https://doi.org/10.1017/9781009157896)
- 857 Ivanovic, R. F. et al.: Acceleration of Northern Ice Sheet Melt Induces AMOC Slowdown and Northern Cooling in
858 Simulations of the Early Last Deglaciation. *Paleoceanography and Paleoclimatology* 33, 807-824.
859 <https://doi.org/10.1029/2017pa003308>, 2018.
- 860 Ivanovic, R. F. et al.: Transient climate simulations of the deglaciation 21-9 thousand years before present (version 1)-
861 PMIP4 Core experiment design and boundary conditions. *Geoscientific Model Development* 9, 2563-2587.
862 <https://doi.org/10.5194/gmd-9-2563-2016>, 2016.
- 863 Izumi, K., Valdes, P., Ivanovic, R. *et al.* Impacts of the PMIP4 ice sheets on Northern Hemisphere climate during the last
864 glacial period. *Clim Dyn* 60, 2481–2499. <https://doi.org/10.1007/s00382-022-06456-1>, 2023.
- 865 Joshi, M. M., Webb, M. J., Maycock, A. C., and Collins, M.: Stratospheric water vapour and high climate sensitivity in a
866 version of the HadSM3 climate model, *Atmos. Chem. Phys.*, 10, 7161–7167, <https://doi.org/10.5194/acp-10-7161-2010>,
867 2010.
- 868 [Leccavalier, B. S., Milne, G. A., Simpson, M. J. R., Wake, L., Huybrechts, P., Tarasov, L., Kjeldsen, K. K., Funder, S., Long,
869 A. J., Woodroffe, S., Dyke, A. S., and Larsen, N. K.: A model of Greenland ice sheet deglaciation constrained by](https://doi.org/10.1017/9781009157896)

870 ~~observations of relative sea level and ice extent, *Quaternary Sci. Rev.*, 102, 54–84,~~
871 ~~<https://doi.org/10.1016/j.quascirev.2014.07.018>, 2014.~~

872 ~~Lee, V., Cornford, S., & Payne, A.: Initialization of an ice sheet model for present day Greenland. *Annals of Glaciology*,~~
873 ~~56(70), 129–140. doi:10.3189/2015AoS70A121, 2015.~~

874 ~~Matero, I. S. O., Gregoire, L. J., and Ivanovic, R. F.: Simulating the Early Holocene demise of the Laurentide Ice Sheet with~~
875 ~~BISICLES (public trunk revision 3298), *Geosci. Model Dev.*, 13, 4555–4577, [https://doi.org/10.5194/gmd-13-4555-](https://doi.org/10.5194/gmd-13-4555-2020)~~
876 ~~2020, 2020.~~

877 ~~Niu, L., Lohmann, G., Hinck, S., Gowan, E. J. & Krebs-Kanzow, U.: The sensitivity of Northern Hemisphere ice sheets~~
878 ~~to atmospheric forcing during the last glacial cycle using PMIP3 models. *Journal of Glaciology* 65, 645–661.~~
879 ~~<https://doi.org/10.1017/jog.2019.42>, 2019.~~

880 ~~Obase, T., A. Abe-Ouchi, K. Kusahara, H. Hasumi, and R. Ohgaito, 2017: Responses of Basal Melting of Antarctic Ice~~
881 ~~Shelves to the Climatic Forcing of the Last Glacial Maximum and CO2 Doubling. *J. Climate*, 30, 3473–3497,~~
882 ~~<https://doi.org/10.1175/JCLI-D-15-0908.1>.~~

883 ~~Ogura, T., Abe-Ouchi, A., and Hasumi, H. (2004), Effects of sea ice dynamics on the Antarctic sea ice distribution in a~~
884 ~~coupled ocean-atmosphere model, *J. Geophys. Res.*, 109, C04025, doi:10.1029/2003JC002022.~~

885 ~~Oishi, R. and Abe-Ouchi, A.: Influence of dynamic vegetation on climate change and terrestrial carbon storage in the Last~~
886 ~~Glacial Maximum, *Clim. Past*, 9, 1571–1587 (2013). <https://doi.org/10.5194/cp-9-1571-2013>~~

887 ~~Pollard, D. A retrospective look at coupled ice sheet–climate modeling. *Climatic Change* 100, 173–194 (2010).~~
888 ~~<https://doi.org/10.1007/s10584-010-9830-9>~~

889 ~~Kachuck, S. B., Martin, D. F., Bassis, J. N., & Price, S. F. (2020).: Rapid viscoelastic deformation slows marine ice sheet~~
890 ~~instability at Pine Island Glacier. *Geophysical Research Letters*, 47, e2019GL086446.~~
891 ~~<https://doi.org/10.1029/2019GL086446>, 2020.~~

892 ~~Kageyama, M. et al. The PMIP4 Last Glacial Maximum experiments: preliminary results and comparison with the PMIP3~~
893 ~~simulations. *Climate of the Past* 17, 1065–1089 (2021). <https://doi.org/10.5194/cp-17-1065-2021>.~~
894 ~~<https://doi.org/10.5194/cp-17-1065-2021>, 2021.~~

895 ~~Kageyama, M. et al. The PMIP4 contribution to CMIP6-Part 4: Scientific objectives and experimental design of the PMIP4-~~
896 ~~CMIP6 Last Glacial Maximum experiments and PMIP4 sensitivity experiments. *Geoscientific Model Development* 10,~~
897 ~~4035–4055 (2017). <https://doi.org/10.5194/gmd-10-4035-2017>. <https://doi.org/10.5194/gmd-10-4035-2017>, 2017.~~

898 ~~Klockmann, M., Mikolajewicz, U. & Marotzke, J. The effect of greenhouse gas concentrations and ice sheets on the glacial~~
899 ~~AMOC in a coupled climate model. *Climate of the Past* 12, 1829–1846 (2016). <https://doi.org/10.5194/cp-12-1829-2016>.~~
900 ~~<https://doi.org/10.5194/cp-12-1829-2016>, 2016.~~

901 ~~Lecavalier, B. S., Milne, G. A., Simpson, M. J. R., Wake, L., Huybrechts, P., Tarasov, L., Kjeldsen, K. K., Funder, S., Long,~~
902 ~~A. J., Woodroffe, S., Dyke, A. S., and Larsen, N. K.: A model of Greenland ice sheet deglaciation constrained by~~
903 ~~observations of relative sea level and ice extent, *Quaternary Sci. Rev.*, 102, 54–84,~~
904 ~~<https://doi.org/10.1016/j.quascirev.2014.07.018>, 2014.~~

905 ~~Lee, V., Cornford, S., & Payne, A.: Initialization of an ice-sheet model for present-day Greenland. *Annals of Glaciology*,~~
906 ~~56(70), 129–140. doi:10.3189/2015AoS70A121, 2015.~~

907 ~~Lofverstrom, M., Liakka, J. & Kleman, J. The North American Cordillera-An Impediment to Growing the Continent-Wide~~
908 ~~Laurentide Ice Sheet. *Journal of Climate* 28, 9433–9450 (2015). <https://doi.org/10.1175/jcli-d-15-0044.1>.~~
909 ~~<https://doi.org/10.1175/jcli-d-15-0044.1>, 2015.~~

910 ~~Manabe, S. & Broccoli, A. J. THE INFLUENCE OF CONTINENTAL ICE SHEETS ON THE CLIMATE OF AN ICE-~~
911 ~~AGE. *Journal of Geophysical Research-Atmospheres* 90, 2167–2190 (1985). <https://doi.org/10.1029/JD090iD01p02167>,~~
912 ~~<https://doi.org/10.1029/JD090iD01p02167>,~~
912 ~~1985.~~

913 [Martin-Margold, M.,](#) Chris R. Stokes, Chris D. Clark, Reconciling records of ice streaming and ice margin retreat to produce
914 a palaeogeographic reconstruction of the deglaciation of the Laurentide Ice Sheet, *Quaternary Science Reviews*, Volume
915 189, 2018, Pages 1-30, ISSN 0277-3791,
916 <https://doi.org/10.1016/j.quascirev.2018.03.013><https://doi.org/10.1016/j.quascirev.2018.03.013>. 2018.

917 Martin, D. F., Cornford, S. L., & Payne, A. J. (2019). Millennial-scale vulnerability of the Antarctic Ice Sheet to regional
918 ice shelf collapse. *Geophysical Research Letters*, 46, 1467–1475. <https://doi.org/10.1029/2018GL081229>, 2019.

919 [Matero, I. S. O., Gregoire, L. J., and Ivanovic, R. F.:](#) *Simulating the Early Holocene demise of the Laurentide Ice Sheet with*
920 *BISICLES (public trunk revision 3298)*, *Geosci. Model Dev.*, 13, 4555–4577, [https://doi.org/10.5194/gmd-13-4555-](https://doi.org/10.5194/gmd-13-4555-2020)
921 [2020](https://doi.org/10.5194/gmd-13-4555-2020), 2020.

922 Murphy, J., Sexton, D., Barnett, D. *et al.* Quantification of modelling uncertainties in a large ensemble of climate change
923 simulations. *Nature* 430, 768–772 (2004). <https://doi.org/10.1038/nature02771>, <https://doi.org/10.1038/nature02771>,
924 2004.

925 NOAA National Centers for Environmental Information (2023). State of the Climate: Global Climate Report for 2022.
926 Accessed January 18, 2023, from <https://www.ncei.noaa.gov/access/monitoring/monthly-report/global/202213>. [Niu, L.,](#)
927 [Lohmann, G., Hinck, S., Gowan, E. J. & Krebs-Kanzow, U.:](#) *The sensitivity of Northern Hemisphere ice sheets to*
928 *atmospheric forcing during the last glacial cycle using PMIP3 models*. *Journal of Glaciology* 65, 645-661.
929 <https://doi.org/10.1017/jog.2019.42>. 2019.

930 [Obase, T., Abe-Ouchi, K. Kusahara, H. Hasumi, and R. Ohgaito.:](#) *Responses of Basal Melting of Antarctic Ice Shelves to*
931 *the Climatic Forcing of the Last Glacial Maximum and CO2 Doubling*. *J. Climate*, 30, 3473–3497,
932 <https://doi.org/10.1175/JCLI-D-15-0908.1>. 2017.

933 [Ogura, T., Abe-Ouchi, A., and Hasumi, H.:](#) *Effects of sea ice dynamics on the Antarctic sea ice distribution in a coupled*
934 *ocean atmosphere model*, *J. Geophys. Res.*, 109, C04025, doi:10.1029/2003JC002022. 2004.

935 [O'ishi, R. and Abe-Ouchi, A.:](#) *Influence of dynamic vegetation on climate change and terrestrial carbon storage in the Last*
936 *Glacial Maximum*, *Clim. Past*, 9, 1571–1587. <https://doi.org/10.5194/cp-9-1571-2013>, 2013.

937 [Pollard, D. and DeConto, R. M.:](#) *Description of a hybrid ice sheet-shelf model, and application to Antarctica*, *Geosci. Model*
938 *Dev.*, 5, 1273–1295, <https://doi.org/10.5194/gmd-5-1273-2012>, 2012.

939 Paul, A., Mulitza, S., Stein, R. & Werner, M. A global climatology of the ocean surface during the Last Glacial Maximum
940 mapped on a regular grid (GLOMAP). *Climate of the Past* 17, 805-824 (2021). <https://doi.org/10.5194/cp-17-805-2021>,
941 <https://doi.org/10.5194/cp-17-805-2021>, 2021.

942 Pico, T., Creveling, J. R. & Mitrovica, J. X. Sea-level records from the US mid-Atlantic constrain Laurentide Ice Sheet
943 extent during Marine Isotope Stage 3. *Nature Communications* 8 (2017). <https://doi.org/10.1038/ncomms15612>, 2017.

944 Pukelsheim, F. The Three Sigma Rule, *The American Statistician*, 48, 88–91, (<https://doi.org/10.2307/2684253>), 1994).
945 <https://doi.org/10.2307/2684253>).

946 Quiquet, A., Roche, D. M., Dumas, C., Bouttes, N., and Lhardy, F.: Climate and ice sheet evolutions from the last glacial
947 maximum to the pre-industrial period with an ice-sheet–climate coupled model, *Clim. Past*, 17, 2179–2199,
948 <https://doi.org/10.5194/cp-17-2179-2021>, 2021.

949 Roche, D. M., Dumas, C., Bügelmayer, M., Charbit, S., and Ritz, C.: Adding a dynamical cryosphere to *iLOVECLIM*
950 (version 1.0): coupling with the GRISLI ice-sheet model, *Geosci. Model Dev.*, 7, 1377–1394,
951 <https://doi.org/10.5194/gmd-7-1377-2014>, 2014.

952 Roe, G. H. & Lindzen, R. S. The mutual interaction between continental-scale ice sheets and atmospheric stationary waves.
953 *Journal of Climate* 14, 1450-1465 (2001). [https://doi.org/10.1175/1520-0442\(2001\)014<1450:tmibcs>2.0.co;2](https://doi.org/10.1175/1520-0442(2001)014<1450:tmibcs>2.0.co;2)

954 Rougier, J., D. M. H. Sexton, J. M. Murphy, and D. Stainforth, (2009). Analyzing the Climate Sensitivity of the HadSM3
955 Climate Model Using Ensembles from Different but Related Experiments. *J. Climate*, 22, 3540–3557,

956 <https://doi.org/10.1175/2008JCLI2533.1>, 2009.

957 Sanderson, B. M., 2011: A Multimodel Study of Parametric Uncertainty in Predictions of Climate Response to Rising
958 Greenhouse Gas Concentrations. *J. Climate*, **24**, 1362–1377, <https://doi.org/10.1175/2010JCLI3498.1>, 2011.

959 Schmittner, A., et al , Climate Sensitivity Estimated from Temperature Reconstructions of the Last Glacial Maximum.
960 *Science* **334**, 1385–1388 (2011). DOI:10.1126/science.1203513, 2011.

961 Sherriff-Tadano, S., Abe-Ouchi, A. & Oka, A.: Impact of mid-glacial ice sheets on deep ocean circulation and global
962 climate. *Climate of the Past* **17**, 95–110. [https://doi.org:10.5194/cp-17-95-2021](https://doi.org/10.5194/cp-17-95-2021), 2021.

963 Sherriff-Tadano, S., Abe-Ouchi, A., Yoshimori, M., Hotta, H., Kikuchi, M., Ohgaito, R., Kodama, T., Vadsaria, T., Oka, A,
964 Suzuki, K.: Southern Ocean surface temperatures and cloud biases in climate models connected to the representation of
965 glacial deep ocean circulation, *Journal of Climate*, (2023).

966 Shiogama, H., Watanabe, M., Yoshimori, M. *et al.*: Perturbed physics ensemble using the MIROC5 coupled atmosphere–
967 ocean GCM without flux corrections: experimental design and results. *Clim Dyn* **39**, 3041–3056.
968 <https://doi.org/10.1007/s00382-012-1441-x>, 2012.

969 Smith, R. S.: The FAMOUS climate model (versions XFXWB and XFHCC): description update to version XDBUA.
970 *Geoscientific Model Development* **5**, 269–276. [https://doi.org:10.5194/gmd-5-269-2012](https://doi.org/10.5194/gmd-5-269-2012), 2012.

971 Smith, R. S., George, S. & Gregory, J. M. FAMOUS version xotzt (FAMOUS-ice): a general circulation model (GCM)
972 capable of energy- and water-conserving coupling to an ice sheet model. *Geoscientific Model Development* **14**, 5769–
973 5787. [https://doi.org:10.5194/gmd-14-5769-2021](https://doi.org/10.5194/gmd-14-5769-2021), 2021.

974 Smith, R. S., Mathiot, P., Siahhan, A., Lee, V., Cornford, S. L., Gregory, J. M., et al.: Coupling the U.K. Earth System model
975 to dynamic models of the Greenland and Antarctic ice sheets. *Journal of Advances in Modeling Earth Systems*, **13**,
976 e2021MS002520. <https://doi.org/10.1029/2021MS002520>, 2021.

977 Smith, R. S. & Gregory, J.: The last glacial cycle: transient simulations with an AOGCM. *Climate Dynamics* **38**, 1545–1559.
978 [https://doi.org:10.1007/s00382-011-1283-y](https://doi.org/10.1007/s00382-011-1283-y), 2012.

979 Smith, R. S., Gregory, J. M. & Osprey, A.: A description of the FAMOUS (version XDBUA) climate model and control run.
980 *Geoscientific Model Development* **1**, 53–68. [https://doi.org:10.5194/gmd-1-53-2008](https://doi.org/10.5194/gmd-1-53-2008), 2008.

981 Smith, R.N.B.: A scheme for predicting layer clouds and their water content in a general circulation model. *Q.J.R. Meteorol.*
982 *Soc.*, **116**: 435–460. <https://doi.org/10.1002/qj.49711649210>, 1990.

983 Tabone, I., Blasco, J., Robinson, A., Alvarez-Solas, J., and Montoya, M.: The sensitivity of the Greenland Ice Sheet to
984 glacial–interglacial oceanic forcing, *Clim. Past*, **14**, 455–472, <https://doi.org/10.5194/cp-14-455-2018>, 2018.

985 Tarasov, L., Dyke, A. S., Neal, R. M. & Peltier, W. R.: A data-calibrated distribution of deglacial chronologies for the North
986 American ice complex from glaciological modeling. *Earth and Planetary Science Letters* **315**, 30–40.
987 [https://doi.org:10.1016/j.epsl.2011.09.010](https://doi.org/10.1016/j.epsl.2011.09.010), 2012.

988 Tierney, J. E. et al.: Glacial cooling and climate sensitivity revisited. *Nature* **584**, 569+. [https://doi.org:10.1038/s41586-020-2617-x](https://doi.org/10.1038/s41586-020-2617-x), 2020.

990 Tsai, V., Stewart, A., & Thompson, A.: Marine ice-sheet profiles and stability under Coulomb basal conditions. *Journal of*
991 *Glaciology*, **61**(226), 205–215. doi:10.3189/2015JoG14J221, 2015.

992 van de Wal, R. S. W., Boot, W., Smeets, C. J. P. P., Snellen, H., van den Broeke, M. R., and Oerlemans, J.: Twenty-one
993 years of mass balance observations along the K-transect, West Greenland, *Earth Syst. Sci. Data*, **4**, 31–35,
994 <https://doi.org/10.5194/essd-4-31-2012>, 2012.

995 Van Liefferinge, B., Taylor, D., Tsutaki, S., Fujita, S., Gogineni, P., Kawamura, K., et al.: Surface mass balance controlled
996 by local surface slope in inland Antarctica: Implications for ice-sheet mass balance and Oldest Ice delineation in Dome
997 Fuji. *Geophysical Research Letters*, **48**, e2021GL094966. <https://doi.org/10.1029/2021GL094966>, 2021.

998 Vizcaino, M. et al.: Greenland Surface Mass Balance as Simulated by the Community Earth System Model. Part I: Model

999 Evaluation and 1850-2005 Results. *Journal of Climate* 26, 7793-7812. <https://doi.org:10.1175/jcli-d-12-00615.1>, 2013.

.000 Williamson, D. Exploratory ensemble designs for environmental models using k-extended latin hypercubes. *Environmetrics*,

.001 26 (4), 268–283 (2015). <https://onlinelibrary.wiley.com/doi/full/10.1002/env.2335>

.002 Williams, K. D., Senior, C. A. and Mitchell, J. F. B.: Transient Climate Change in the Hadley Centre Models: The Role of

.003 Physical Processes. *J. Climate*, **14**, 2659–2674, [https://doi.org/10.1175/1520-0442\(2001\)014<2659:TCCITH>2.0.CO;2](https://doi.org/10.1175/1520-0442(2001)014<2659:TCCITH>2.0.CO;2),

.004 2001.

.005 Willeit, M. & Ganopolski, A.: The importance of snow albedo for ice sheet evolution over the last glacial cycle. *Climate of*

.006 *the Past* 14, 697-707. <https://doi.org:10.5194/cp-14-697-2018>, 2018.

.007 Yamagishi, T., Abe-Ouchi, A., Saito, F., Segawa, T., & Nishimura, T.: Re-evaluation of paleo-accumulation

.008 parameterization over Northern Hemisphere ice sheets during the ice age examined with a high-resolution AGCM and a

.009 3-D ice-sheet model. *Annals of Glaciology*, **42**, 433-440. doi:10.3189/172756405781813032, 2005.

.010 Ziemen, F. A., Rodehacke, C. B., and Mikolajewicz, U.: Coupled ice sheet–climate modeling under glacial and pre-industrial

.011 boundary conditions, *Clim. Past*, **10**, 1817–1836, <https://doi.org/10.5194/cp-10-1817-2014>, 2014.

.012 Zhu, J., Otto-Bliesner, B., Brady, E., Poulsen, C.J., Shaw, J.K., Kay, J.E. LGM paleoclimate constraints inform cloud

.013 parameterizations and equilibrium climate sensitivity in CESM2. *Journal of Advances in Modeling Earth Systems*, **14**(4),

.014 e2021MS002776. <https://doi.org/10.1029/2021MS002776>, 2022.

.015 Zhu, J. and Poulsen, C. J.: Last Glacial Maximum (LGM) climate forcing and ocean dynamical feedback and their

.016 implications for estimating climate sensitivity, *Clim. Past*, **17**, 253–267, <https://doi.org/10.5194/cp-17-253-2021>, 2021.

.017